EXPERIMENTAL STUDY OF HELIUM AND ARGON DIFFUSION IN THE WAKE OF A CIRCULAR CYLINDER AT M = 5.8

Thesis by

Louis Kingsland, Jr.

In Partial Fulfillment of the Requirements

For the Degree of

Aeronautical Engineer

California Institute of Technology

Pasadena, California

1961

ACKNOWLEDGMENTS

The author wishes to express his appreciation to Professor Lester Lees, Dr. Toshi Kubota and Dr. Edward Zukoski for their guidance during the course of the investigation. He also wishes to thank Mr. Paul Baloga and staff of the hypersonic laboratory for their expert assistance in the conduct of the experiments, Mrs. Truus van Harreveld for doing the computations, Mrs. Betty Wood for preparing the figures, and Mrs. Geraldine Van Gieson for typing the manuscript.

ABSTRACT

Experimental measurements of the diffusion of helium and argon in the wake of a porous cylinder were made in the GALCIT hypersonic wind tunnel at Mach number 5.8. The cylinder was mounted perpendicular to the flow and small quantities of tracer gas were pumped through the model walls into the flow. The thermal conductivity method of gas analysis was used to determine the concentration of sample gases extracted from points in the wake.

The transverse and axial distribution of concentration appeared to follow theoretical estimates of "similarity behavior". Injection of tracer gas was found to have a measurable effect on stagnation pressure and this effect was taken into account during computations. Numerical values of diffusion coefficients along the wake centerline were computed from the experimental data and then compared with theoretical values for laminar flow. Close agreement between experimental and theoretical values at $Re_d = 18,000$ verified that the inner wake was laminar as far downstream as measurements could be made (15 diameters). At $Re_d = 72,000$, the data showed that mixing processes were 3 times more rapid for helium, and 10 times more rapid for argon, than those expected in laminar flow. This result confirmed the presence of turbulence at this flow condition.

TABLE OF CONTENTS

LIST OF TABLES AND FIGURES

LIST OF SYMBOLS

a	speed of sound
a_2, a_4	constants
b	cylinder span
b_2, b_4	constants
c_p	specific heat at constant pressure
c_v	specific heat at constant volume
D_k	general mass diffusion coefficient
D_{12}	binary diffusion coefficient
D_T	turbulent mass diffusion coefficient
d	cylinder diameter
E	voltage
I	electrical current
K_i	mass fraction of i^{th} component
k_T	ratio of thermal and binary diffusion coefficients
$\mathcal{M}$	molecular weight
M	Mach number
$\dot{m}$	mass flow rate
N_i	mole fraction of i^{th} component
n_i	number of moles of i^{th} component
P	static pressure
P_o	stagnation pressure in the tunnel reservoir
P_t	stagnation pressure in the flow
R_i	gas constant of i^{th} component
R_o	universal gas constant
Re	Reynolds number

T	static temperature
T/C	thermal conductivity cell
T_o	stagnation temperature in tunnel reservoir
t	time
u	axial velocity component
V	volume
v	vertical velocity component
x	axial coordinate, rearward from cylinder center
y	vertical coordinate, upward from cylinder center
Y	transformed vertical coordinate
γ	ratio of specific heats
Δ	denotes incremental quantity
μ	viscosity
ρ	density

Subscripts

A	refers to argon
bar	refers to barometric conditions
$\mathfrak{L}$	refers to conditions at wake centerline ($y = 0$)
e	refers to flow quantities in the outer wake
He	refers to helium
i	refers to i^{th} component
o	refers to reservoir conditions
1	refers to conditions ahead of the probe shock wave
2	refers to conditions behind the probe shock wave

I. INTRODUCTION

With the advent of mass injection and ablation from a body during re-entry, the diffusion of mass in the wake of bodies in hypersonic flow has become of great practical interest. This interest is based, to a large extent, on concern with the radar reflectivity and radiative emissivity of materials in the wake. Any study of this subject requires a basic understanding of the distribution of the material in the wake, or in other words, of the mass diffusion processes. In addition to questions of the material distribution, the study of the wake mass diffusion is closely connected with the diffusion of momentum and energy in the wake.

This experimental investigation constitutes the second phase of a general study at GALCIT of the diffusion of mass in the wake of a cylinder in hypersonic flow. The first phase consisted of an investigation by W. Mohlenhoff[10]* of the effectiveness of the thermal conductivity method of gas analysis for determining the concentration of helium in a hypersonic wake. His investigation demonstrated that this method was quite satisfactory and would be very effective in studies of diffusion at hypersonic speeds. His discussion of the detailed experimental procedures and his recommendations for equipment modification were very helpful to the author in the preparation of the present experimental study. Mohlenhoff's paper also contained a good resume of previous work and references pertinent to the subject.

The basic steps in the gas analysis method employed in this

---

* Superscripts denote references listed at end of text.

experiment were:

(1) Controlled injection of a tracer gas from a model in hypersonic flow.

(2) Extraction of gas samples from points in the wake by means of a fine probe.

(3) Collection of these samples in a T/C (thermal conductivity) gas analysis cell.

(4) Conversion of the T/C cell reading into a meaningful value of gas composition.

In the discussion of these basic steps and the equipment involved (Section II) a great deal of material which has already been well covered in the previous work by Mohlenhoff need not be repeated here. However, those particulars which had to be modified or which presented special problems will be discussed in sufficient detail.

The first objective of the present investigation was to modify the existing equipment and procedures so as to increase the precision and speed of the data-taking process, which had been a major problem in the previous investigation. The next objective was to obtain sufficient data concerning the diffusion of helium to permit numerical evaluation of the diffusion coefficients and comparison with theoretical predictions, where possible. Finally, it was desired to obtain comparable data for the diffusion of a heavier gas, such as argon, to determine the effect of molecular weight on diffusion processes, especially in turbulent flow.

II. EXPERIMENTAL APPARATUS AND PROCEDURE

II. 1. Wind Tunnel Description

All tests in this investigation were performed in Leg 1 of the GALCIT hypersonic wind tunnel, which is a closed return, continuously operating tunnel. Leg 1 has fixed nozzle blocks which provide a nominal test section Mach number of 5.8. It is capable of operation with reservoir pressure, P_o, between -5 and + 100 psig and reservoir temperature, T_o, between 225° and 325°F. The test section has cross sectional dimensions of 5" by 5.25" and the test rhombus theoretically extends 29" in the axial direction. In reality, however, there exist small disturbances, originating mostly in the throat region of the nozzle, which amount to $\pm$ 5 per cent variation in pitot pressure distribution in some regions of the test rhombus. It appears that the flow in the wake of a body is rather sensitive to this non-uniformity, necessitating measurements to be confined to a region extending 4.5 inches in the stream direction at P_o = 10 psig and 8 inches at P_o = 85 psig.

Diffusion measurements in this investigation were made at P_o = 10 psig and at P_o = 85 psig, both at T_o = 275°F. A reservoir pressure of 10 psig was the minimum pressure at which the presence of the model and probe would not cause choking of the flow, and a reservoir pressure of 85 psig was the maximum pressure at which the tunnel could be operated for extended periods of time. The intermittent presence of oil particles in the flow caused considerable difficulty which will be discussed in the next section. These particles apparently originated in the compressors and were carried along with the flow.

So far, attempts to filter or screen out these particles have been unsuccessful.

The Reynolds numbers based on the flow conditions ahead of the bow shock and on the model diameter (0.3") for the two tunnel reservoir conditions utilized in this investigation are:

$$Re_d = 18,000 \text{ at } P_o = 10 \text{ psig}$$
$$T_o = 275^\circ F$$
$$Re_d = 72,000 \text{ at } P_o = 85 \text{ psig}$$
$$T_o = 275^\circ \quad .$$

Previous pressure, hot-wire, and concentration measurements have indicated that at $P_o = 10$ psig, the inner wake is laminar, while at $P_o = 85$ psig, it is turbulent. It was hoped that the present investigation could help determine the validity of these observations, and provide additional information about mass diffusion processes in the wake.

II. 2. Injection of the Tracer Gas

The helium and argon gases used as tracers in this experiment were supplied from high pressure commercial gas bottles, by throttling through a pressure regulator (Figure 1). Helium was chosen because its thermal conductivity is much larger than that of air (Table 1), and because it is safe to use without drastic precautions against fire or atmospheric poisoning. Argon was chosen as the second tracer gas because it is ten times heavier than helium, and might show behavior considerably different from that of helium because of this greater relative mass. Argon retains the safety of helium, but does not differ from air in thermal conductivity as greatly as helium does.

The injection gas supply was metered through a single Fischer-Porter Tri-flat flowmeter (FP-1/4-16-G-5, with 1/4" glass ball float). This instrument replaced a larger flowmeter and a smaller flowmeter which had been used in series previously. The new flowmeter was checked against performance data supplied by the manufacturer and was found to perform as predicted. This calibration consisted of the displacement of a measured quantity of water by helium metered at atmospheric pressure in a given time interval.

Gas pressure was monitored at both the entrance and exit of the flowmeter with a U-tube mercury manometer. Flow level and metering pressure were adjusted by manipulating throttling valves located on both sides of the flowmeter (Figure 1). Although pressure and flow level were coupled, the valve at the exit of the flowmeter had the most effect on flow rate, while metering pressure was most sensitive to adjustments of the inlet valve. After a given flow rate had been established, small variations in supply pressure could be easily detected by the mercury manometer and controlled by the inlet valve to within $\pm$ 0.5 mm. Hg., resulting in no more than $\pm$ 0.2 per cent deviation in mass flow rate for a fixed flow rate setting. The repeatability of the flow rate setting, however, if it had been disturbed, was poor because the flowmeter could be read with an accuracy no better than $\pm$ 3 per cent. Even over a period of several days, flow rate variations were minute if the flow rate setting remained untouched, and adjustments were made by means of the inlet valve alone. However, if the exit valve was moved or adjusted, the chances of exactly duplicating the previous flow rate were considerably lessened. Therefore, adjustments

in the setting of this valve were pointedly avoided after the desired flow rate had been established.

II. 3. Cylindrical Model

The model used in this investigation was a 0. 30" diameter porous circular cylinder, with an exposed length of 5" from wall to wall in the wind tunnel test section. It was mounted horizontally across the tunnel 17. 34 inches downstream from the throat. The dimensions of the model are identical to those used by Mohlenhoff[10], and to those presently being used in total pressure and static pressure surveys by McCarthy. By keeping dimensions the same, it was expected that diffusion measurements could be correlated with pressure measurements already available.

The present model was similar to those used by Mohlenhoff in that it was composed of a porous alumina material. The alumina composition was slightly different, making it considerably less brittle, so that the breakage problem, which had plagued previous efforts, was negligible. In addition, the interior diameter, 0. 065", was about half that of previous models.

The method of sealing and holding the model ends in place by clamping and locking with soft "O"-rings was found to be cumbersome. This technique was replaced by fitting small diameter tubing into both ends of the model and bonding the tubing to the model with an epoxy resin, which also served as an effective seal. The tracer gas was pumped into the model through this tubing (Figure 2). In addition, the ends of the model, which were held in the tunnel walls during operation,

were coated and sealed with this resin to eliminate any tracer gas ejection from regions other than the surface exposed to the flow. A new clamping and locking arrangement, using threaded hollow bolts, held the model in place with soft "O"-rings. These "O"-rings were not necessary for preventing helium leakage, but served to cushion the model and to prevent leakage of outside air into the tunnel (Figure 2).

Considerable difficulty was encountered during the course of the investigation when it was found that concentration levels obtained in the wake did not agree with the amount of helium being injected into the model, but were consistently about 50 per cent to 75 per cent of the expected value. This discrepancy was determined by integrating the mass flow of helium across the wake in the center vertical plane of the test section. (This computation is discussed in detail in Section III. 1.) This discovery resulted in a complete shakedown and recalibration of the entire experimental setup, which led to the conclusion that injection of the gas from the model was not uniform.

By immersing various models in water, pumping helium through them, and observing the ejection rates along the length of their surfaces, it was found that models which had not been used in the tunnel displayed fairly uniform ejection rates along their entire lengths. Models which had been used in the tunnel, however, when tested in the same way, were found to have very high ejection rates at the model ends and considerably lower rates along the remainder of the length. Unused models which had been determined to be uniform in ejection rates, were installed in the tunnel flow for a period of time, then taken out and checked. After exposure to tunnel flow conditions, they too displayed

the non-uniform ejection pattern described above.

Visual examination of these models showed that, after running in the tunnel, they had become coated with the oil which is present intermittently in the flow. The impact and flow rate of these oil particles in the flow is apparently greatest in the center of the flow, i. e., in the region away from the low-speed wall boundary layer. Thus, the central portions of the models were considerably more saturated with oil than were the ends of the models.

During water immersion tests, many models displayed non-uniform ejection rates along their center portions, which may be attributed to irregular model composition or porosity. Several models were found, however, which displayed very uniform ejection rates over their entire center sections, with non-uniformities confined to that region of the model surface exposed to the boundary layer. Because of the relatively slow diffusion times, any gas ejected at the very ends of the model would not be expected to diffuse into the center section until far downstream of the test section. Even at the location of the rear-most diffusion profiles, $x/D = 24$, it was found that the tracer gas had not diffused more than 0.3" vertically from the centerline, and the same order of magnitude of diffusion distance could be expected for any cross-diffusion from the boundary layer, which was 2.5" from the centerline.

One particularly uniform model was selected and then subjected to repeated testing in the tunnel and in water immersion over a period of a month, to determine if any significant changes in ejection pattern would take place. Pressure and concentration profiles were repeatedly taken over this period in the vertical center plane and at several down-

stream positions. Integration of the mass flow at each of these positions showed practically no change in the total amount of tracer gas flow in the vertical center plane between successive downstream positions. This result proved that the excess mass being injected into the boundary layer was not diffusing into the test section. Repeated testing of the model by water immersion during this period also showed no significant change in surface ejection pattern. All diffusion data in this report was obtained from tests with this model.

II. 4. Tracer Gas Injection Rates

Initially, the helium flow rate used in this experiment was 0. 003 lb/min, which is the same as that used by Mohlenhoff[10]. Because the present equipment is much more sensitive, a much smaller flow rate of helium could be readily measured. In addition, it was learned that the injection of gas from the model had a noticeable effect on total pressure values in the wake (Section III. 3.), so a helium flow rate of approximately 0. 0004 lb/min was chosen as an adequate level. This flow rate represented the minimum level which could be accurately controlled by the flowmeter.

The T/C cell was somewhat less sensitive to a given mole fraction of argon than it was to the same mole fraction of helium (Figure 6). In addition, the molecular weight of argon is ten times that of helium, so that it was necessary to inject argon at a mass flow rate about twenty-five times that of helium, or 0. 010 lb/min, when the tunnel reservoir pressure, P_o , was 85 psig. At the lower pressure, P_o = 10 psig, the same mass flow rate yielded much higher concentra-

tions, so the argon injection rate was cut down to 0.005 lb/min, to reduce the effect of argon injection on total pressure in the wake.

II.5. Probe

The probe used to extract gas samples from the flow had a tip made of flattened hypodermic tubing with an orifice width of 0.04" and a height of 0.004". The thickness of the tubing walls was 0.004", resulting in overall tip frontal dimensions of 0.048" by 0.012". This probe was used for the measurement of both concentration and total pressure. It was mounted in a traverse mechanism which could move the probe axially from zero to ten inches downstream of the model within $\pm$ 0.005", and vertically from 1.5" below to 1.2" above the tunnel centerline, within $\pm$ 0.0005".

II.6. Thermal Conductivity Cell

The sample gas was led from the probe into a T/C (thermal conductivity) cell. A short summary of the principle of a T/C cell will be given here, but the reader is referred to works by Daynes[2], Rush and Forstall[13], and Mohlenhoff[10] for a more detailed discussion.

The T/C cell used in this experiment was a GOW-MAC Type 9285, identical to that used by Mohlenhoff. It consisted of two chambers, one containing dry air as a reference and the second containing the sample gas of unknown composition. Four filaments, two in each chamber, were connected to form a Wheatstone bridge (Figure 3). A constant current of 80 m.a. was maintained in the bridge at all times. The voltage across the bridge was balanced at the null position by

filling both chambers with dry air and adjusting a small voltage divider so that voltage across the bridge was zero. The presence of a trace of helium or argon in a new sample gas will cause the thermal conductivity of the sample to be different from that of pure dry air. This variation in thermal conductivity will change the equilibrium temperature of the filaments in the sample gas chamber, resulting in a change in the resistance of the filaments. Since total bridge current is held constant, the entire cell will be slightly unbalanced by these changes, so that a new equilibrium position will be reached. At this new equilibrium position, there will be a small voltage deflection across the bridge, caused by a net change in voltage across each filament. In this way, the cell can be calibrated so that a given bridge voltage deflection can be interpreted as a concentration of helium or argon in a binary mixture with air.

By varying bridge current for a fixed sample gas, and measuring the resulting bridge voltage deflection, it was found that empirically $E_B \sim I_B^{3.5}$, where E_B and I_B are bridge voltage and current, respectively. This fact pointed out that bridge current should be as large as possible for maximum sensitivity, but that a small error in current would produce a proportionately larger error in voltage. The current was limited, however, by the danger of burning out the filament with too large a current. This danger was most severe when the cell was evacuated, because the heat dissipation by thermal conduction would then be least. Bridge current was fixed at 80 m.a., which had been found to be the safe operating limit from past experience at GALCIT with this type of cell.

The sensitivity of bridge voltage to current demanded an extremely precise current control. Bridge current was supplied from two 1.5 volt dry cells in series. Small changes in cell filament resistance, caused by changes in sample gas concentration, resulted in fluctuations in bridge current which had to be detected and controlled. Bridge current was monitored by measuring the voltage across a 0.7 ohm precision resistor which was connected in series with the T/C cell. This voltage was measured with a small potentiometer which could read up to 64 millivolts within $\pm$ 0.004 millivolts. Voltage across the resistor was 56 mv. Therefore bridge current could be held constant within $\pm$ 0.007 per cent, which led to a negligible bridge voltage error of no more than $\pm$ 0.025 per cent. A variable resistor was installed in the circuit to permit these fine current adjustments (Figure 3).

The very low pressure of the samples extracted from the flow created special problems in the measurement of concentration, because the thermal conductivity of a sample gas is a function of its pressure as well as its temperature and composition. A calibration curve was experimentally constructed to correct bridge voltage for the effect of low gas sample pressures (Figure 7). At extremely low pressures, of the order of several millimeters of mercury absolute, the size of this correction and the increasing scatter of calibration points made it all but impossible to use. To avoid this large correction, it became necessary to compress the sample gas to a more favorable pressure. This compression was done by collecting the sample gas in a 100 cc glass bulb adjacent to the thermal conductivity cell (Figure 4), and then compressing the gas into the cell by means of a mercury pump. By

minimizing the volume of the lines and cell connections, a compression ratio of fifteen to one was achieved. The gas pressure was measured by means of an integral U-tube mercury manometer.

The bridge voltage was measured on a Leeds and Northrup K-2 potentiometer, with galvanometer and standard cell, which was capable of accurately determining voltage to four significant figures, and of measuring voltage variations as low as one-half microvolt.

II. 7. Thermal Conductivity Cell Calibration

In order to convert bridge voltage reading into meaningful concentration data the cell must be precisely calibrated. The calibration samples were prepared by thorough mixing of accurately known amounts of helium or argon and dry air. Initially, the procedure used by Mohlenhoff was followed; namely, throttling quantities of high pressure nitrogen into a bottle of helium and accurately measuring the pressure of the helium bottle before and after the addition of nitrogen. Nitrogen had been used because it was more readily available than high pressure dry air. Because nitrogen has only 0.4 per cent less thermal conductivity than dry air, this difference should give negligible error if nitrogen is also used in the reference cavity during calibration.

When the previously mentioned discrepancies in the helium flow rate appeared (Section II. 3.), it was decided to build equipment which could produce more precise mixtures of helium and air for calibration purposes, in order to remove suspicion of error from the calibration. The mixing apparatus consisted of two glass bulbs, connected in such a way that they could be evacuated and filled with accurate quantities

of gases to be mixed, and of tubing, valves and mercury pumps to facilitate the mixing of the gases (Figure 5). The volumes of the bulbs were accurately determined by repeatedly filling them with water up to fixed graduations on the bulbs and measuring the volume of water in graduated cylinders.

During the collection of the gases to be mixed, each bulb was evacuated and then filled with either helium or dry air. Dry air was obtained from the wind tunnel reservoir and collected in gas pressure bottles for use in calibration. Dry air was also used at all times in the reference cavity of the T/C cell. During the collection of the gas in each bulb, adequate time was allowed for the temperature to stabilize, and then gas pressure was measured with a U-tube mercury manometer, which had been evacuated to prevent contamination, before introduction of the new gas.

When each bulb had been sealed off with its known quantity of helium or dry air, all connecting lines between the bulbs were evacuated. Then stopcocks on each bulb were opened, so that the gas in each would be free to diffuse into the other. The mercury pump on each bulb accelerated the mixing process by pumping the gas alternately from one bulb into the other. By repeating this cycle a number of times, a thorough mixing could be expected. After the mixing process, the gas from each bulb was pumped into the sample chamber of the T/C cell at atmospheric pressure, and the bridge voltage was recorded. The voltages resulting from the mixtures in both bulbs were consistently identical, indicating that the mixing process had been complete.

The mole fraction, N_i , of each component in the mixture is

determined from the pressure and volume of each gas before mixing by means of the equation of state for a perfect gas:

$$p = \rho R_o T / \mathcal{M} .$$

The total number of moles, n, in a volume V is

$$n = \rho V / \mathcal{M} = pV / R_o T .$$

Since $T_{He} = T_{Air}$ before mixing, the mole fraction of each component after mixing is

$$N_{He} = \frac{n_{He}}{n_{Air} + n_{He}} = \frac{p_{He} V_{He}}{P_{He} V_{He} + P_{Air} V_{Air}}$$

$$N_{Air} = \frac{n_{Air}}{n_{Air} + n_{He}} = 1 - N_{He} .$$

P_{He}, V_{He}, P_{Air}, and V_{Air} are the pressure and volume of the designated gas in each bulb measured before mixing began.

After completing the calibration for helium-air mixtures in this manner, the resulting data was superimposed on the calibration curve which had been obtained earlier for helium-nitrogen mixtures. There was no measurable difference between the two calibrations, indicating that the first method, although comparatively crude, was quite adequate. The calibration curve for argon-air mixtures was obtained in similar fashion with the new mixing equipment (Figure 6).

If bridge voltage is plotted against the mole fractions of helium or argon in air the resulting curve is closely approximated by a simple polynomial (Figure 6). In addition, the variation of voltage with mole fraction was almost linear in the range of low concentrations, where

most of the experimental tunnel data was obtained.

II. 8. Data Handling

After the voltage across the T/C cell bridge had been read, several intermediate steps were necessary before the reading could be converted into a value of tracer gas mass fraction. When the sample gas pressure was less than one atmosphere, the correction to the voltage (Figure 7) had to be added to the reading. Within the accuracy of the calibration, this voltage correction was found to be independent of the gas composition when the tracer gas mass fraction was less than 25 per cent. The corrected voltage was converted into a mole fraction of tracer gas by means of empirical formulas which were derived from the calibration curves (Figure 6):

$$N_{He} = 4.98 \times 10^{-3} + 5.625\ E^3 \times 10^{-7}$$

$$N_A = 2.15\ E \times 10^{-2} - 8.06\ E^2 \times 10^{-5} \quad .$$

The accumulation of injected tracer gas in the tunnel air supply caused the buildup of a background concentration of this gas. However, leakage of old air and introduction of fresh dry air during each recirculation cycle kept this background concentration down to about 2 per cent of the maximum concentrations measured. This background concentration also included minute, indeterminate amounts of water vapor and other atmospheric vapors which might slowly vary throughout the day. The effect of this variable background concentration was measured by extracting a gas sample at a point outside the viscous wake which had not yet been reached by direct diffusion of the tracer

gas injected from the model. This background effect was monitored at twenty to thirty-minute intervals throughout the day. Since the principal constituent of this background concentration was recirculated tracer gas, the background voltage reading was corrected and converted into an effective background mole fraction of tracer gas. The traces of other vapors were so minute that their effect was assumed to be linearly additive. This effective background mole fraction was subtracted from the total measured mole fraction to yield the mole fraction produced by direct diffusion of the injected tracer gas.

In order to convert the mole fraction of tracer gas into a mass fraction, the following relationship was used:

$$K_1 = (N_1 M_1) / (N_1 M_1 + N_{Air} M_{Air}) ,$$

where

N_1 , N_{Air} = mole fractions of tracer gas and air, respectively

M_1 , M_{Air} = molecular weights of tracer gas and air, respectively

K_1 = mass fraction of tracer gas.

By introducing the values for molecular weight and simplifying, the equations for helium and argon, respectively, are:

$$K_{He} = (N_{He}) / (7.24 - 6.24 N_{He})$$
$$K_A = (N_A) / (0.724 + 0.276 N_A) .$$

II. 9. Pressure Measuring Apparatus

Total pressure and static pressure surveys in the wake of a 0.3" circular solid brass cylinder are the subject of a parallel investigation being carried out by J. McCarthy. It was hoped that pressures

in the wake behind the porous model would correspond to those being obtained by McCarthy, so that diffusion and pressure data could be combined to compute diffusion parameters. It was not expected that all pressure data obtained with the solid cylinder would be repeated for the porous cylinder for purposes of comparison, but if several profiles of total pressure were found to be identical, identical pressure distributions could be assumed with reasonable assurance.

The total pressure in the flow was measured by means of a total pressure probe, connected to a mercury manometer, which was capable of measuring pressures up to one atmosphere within an accuracy of $\pm$ 0.002 cm Hg. The micromanometer was considerably slower than more rapid transducers available, but it was necessary to sacrifice this speed to gain the ability to detect small variations in total pressure caused by the injection of helium or argon.

III. RESULTS AND DISCUSSION

III. 1. Pressure Measurements

A survey of total pressure along the axial centerline (Figure 8) and several total pressure profiles were completed. A comparison of the profiles with those obtained by J. McCarthy behind a solid 0.3" cylinder is presented in Figure 9. Static pressure measurements in the wake of a solid 0.3" cylindrical model had also been made by McCarthy (Figure 13). From this data, Mach number, static temperature, and density profiles were computed.

III. 2. Continuity of Tracer Gas

Before the diffusion data obtained in this investigation could be utilized, it was necessary to determine whether the diffusion processes in the test section were two-dimensional. If the gas ejection from the model is ideally two-dimensional, the mass flow of tracer gas should be identical in every plane perpendicular to the model axis. As explained in Section II. 3., this was not the case. Instead, large ejection rates occurred at the model ends in the tunnel wall boundary layer, with lower ejection rates along the major portion of the model. Bench tests had shown that the ejection rates appeared constant along the surface of the middle portion of the model, but it was necessary to verify this uniformity more precisely.

The mass flow rate was measured at 5, 9, and 15 diameters downstream of the model by taking concentration and total pressure profiles in the center vertical plane at these stations. If the amount of

tracer gas in that vertical plane remained constant between stations, the mass flow rates at all stations would have to be the same. The mass flow rate of tracer gas per unit span at any station can be found by evaluating the integral:

$$\int_{-\infty}^{\infty} \rho u K \, dy \quad .$$

Density cannot be directly measured easily in hypersonic flow, but it can be determined by means of the equation of state if temperature and pressure are known. Static temperature is also difficult to determine, and accurate measurements of static temperature would have involved an effort beyond the scope of this investigation. By assuming isoenergetic flow, the static temperature, T, can be determined within $\pm$ 10 per cent from the equation:

$$T = T_o \Big/ \left(1 + \frac{\gamma - 1}{2} M^2 \right) \quad .$$

The Mach number is then calculated from the total pressure and static pressure data by means of the Rayleigh pitot equation:

$$\frac{P_{t_2}}{P_1} = \left(\frac{\gamma + 1}{2} M_1^2 \right)^{\gamma/(\gamma-1)} \left(\frac{\gamma + 1}{2 M_1^2 - (\gamma - 1)} \right)^{1/(\gamma-1)}$$

Since tracer gas concentration is not constant, the ratio of specific heats, γ , is a variable. For a binary mixture of gases, the ratio of specific heats is given by

$$\gamma = \frac{c_p}{c_v} = \frac{c_{p_1} K_1 + c_{p_2} K_2}{c_{v_1} K_1 + c_{v_2} K_2} \quad .$$

The numerical values for the specific heats are:

$$c_{v_{Air}} = 4,290 \text{ ft}^2/\text{sec}^2\ ^\circ\text{R} \quad , \quad c_{p_{Air}} = 6,006 \text{ ft}^2/\text{sec}^2\ ^\circ\text{R}$$

$$c_{v_{He}} = 18,657 \text{ ft}^2/\text{sec}^2\ ^\circ\text{R} \quad , \quad c_{p_{He}} = 31,095 \text{ ft}^2/\text{sec}^2\ ^\circ\text{R}$$

$$c_{v_{A}} = 1,866 \text{ ft}^2/\text{sec}^2\ ^\circ\text{R} \quad , \quad c_{p_{A}} = 3,110 \text{ ft}^2/\text{sec}^2\ ^\circ\text{R}$$

By substituting these numerical values into the relation for γ and using the relation

$$K_1 + K_2 = 1 \ ,$$

the ratios of specific heats for helium-air and argon-air mixtures, respectively, are expressed as follows:

$$\gamma = \frac{1.4 + 5.85\ K_{He}}{1 + 3.35\ K_{He}}$$

$$\gamma = \frac{1.4 - 0.675\ K_{A}}{1 - 0.565\ K_{A}}$$

Velocity, u , was determined from the equation

$$u = Ma$$

where $a = \sqrt{\gamma RT}$ = speed of sound in a perfect gas. The "gas constant", R , was also a variable, and had to be determined from the equation for R in a binary mixture:

$$R = K_1 R_1 + K_2 R_2 \quad .$$

The numerical values of the gas constant are

$$R_{Air} = 1,716 \text{ ft}^2/\text{sec}^2\ ^\circ\text{R}$$

$$R_{He} = 12,438 \text{ ft}^2/\text{sec}^2\ ^\circ\text{R}$$

$$R_{A} = 1,244 \text{ ft}^2/\text{sec}^2\ ^\circ\text{R} \quad .$$

The gas constants for helium-air and argon-air mixtures are, respectively:

$$R = 1,716 + 10,722\, K_{He}$$

$$R = 1,716 - 472\, K_{A} \quad .$$

Computed $\rho u K$ profiles were plotted (Figures 14, 15, and 16) and integrated over the vertical coordinate, y, for helium concentration data taken during the final model shake-down period at P_o = 85 psig, and at x/d = 5, 9, and 15. Helium mass flow between stations in the vertical center plane remained constant within experimental error. This mass flow corresponded to approximately 60 per cent of the value that would be obtained with an ideally two-dimensional gas ejection. Tracer gas continuity profiles were computed for data taken during the final concentration survey, in the same manner described above, for both helium and argon injection at P_o = 85 psig. The results (Figures 17 and 18) again showed that mass flow remained uniform between stations within the experimental error.

III. 3. Effect of Tracer Gas Injection on Total Pressure

The increase in probe total pressure, Δp_{t_2}, produced by tracer gas injection, relative to probe total pressure without gas injection, p_{t_2}, was measured along the centerline. At P_o = 10 psig, the effect on total pressure by helium injection was most noticeable (Figure 10), but with argon injection, this effect was considerably smaller (Figure 11). At P_o = 85 psig, the effect of helium injection could still be measured, (Figure 12), but it was not possible to detect

any effect caused by argon injection at this reservoir pressure condition.

When $M_1 >> 1$, and $(\rho_1/\rho_2) << 1$, $p_{t_2} \cong \rho_1 u_1^2$. Therefore, total pressure will be affected by changes in either density or velocity. It was expected that velocity would be decreased by gas injection because the tracer gas would have initially less momentum than would the other gases in the flow. Density would be decreased by helium injection, but increased by argon injection, (assuming no change in temperature or static pressure) because of the difference in molecular weights of these gases relative to that of air.

From the experimental plots, the defect in total pressure in the case of helium injection was considerably greater than that in the case of argon injection, but in both cases the injection of tracer gas reduced probe total pressure. This effect was considered in all computations involving total pressure, by measuring total pressure values at the tracer gas injection rates used in the concentration measurements. These values of total pressure taken along the centerline are plotted in Figure 8.

III. 4. Diffusion of Mass in a Laminar Wake

In a steady, laminar, non-reacting hypersonic wake, the diffusion equation takes the form:

$$\rho u \frac{\partial K_i}{\partial x} + \rho v \frac{\partial K_i}{\partial y} = \frac{\partial}{\partial y}\left[\rho D_{12}\left(\frac{\partial K_i}{\partial y} + \frac{\mathcal{M}_1 \mathcal{M}_2}{\mathcal{M}^2} \frac{k_T}{T} \frac{\partial T}{\partial y}\right)\right] .$$

An exact, explicit solution for K_i in a hypersonic wake with large velocity and temperature gradients has not yet been found. As

Mohlenhoff[10] showed, far downstream of the neck where $u \cong u_e$, $T \cong T_e$, and $v \cong 0$, the diffusion equation can be considerably simplified:

$$\rho u_e \frac{\partial K_i}{\partial x} = \frac{\partial}{\partial y}\left[\rho D_{12} \frac{\partial K_i}{\partial y} \right] .$$

By introducing the Howarth-Dorodnitsyn variable:

$$Y = \int_0^y (\rho/\rho_e)\, dy ,$$

and using the theoretical relation:

$$\rho^2 D_{12} \sim (1 / \sqrt{T}) \sim \text{constant} ,$$

the equation becomes: $u_e (\partial K_i/\partial x) = D_{12_e} (\partial^2 K_i/\partial Y^2)$.

The boundary conditions on K_i are

(1) $K_i \longrightarrow 0$ as $y \longrightarrow \infty$

(2) $\int_{-\infty}^{\infty} \rho u K_i \, dy$ = mass flow of tracer gas per unit span = constant = $\dot{m}_i/b$.

A solution of the simplified diffusion equation satisfying the boundary conditions is

$$K_i \cong \frac{\dot{m}_i}{\rho_e u_e b} \sqrt{\frac{u_e}{4\pi D_{12_e} x}} \exp(- u_e Y^2 / 4 D_{12_e} x)$$

This solution indicates the general appearance of diffusion behavior. First of all, the maximum concentration is located along the centerline and decays with downstream distance as follows:

$$K_{\mathcal{L}} \cong \frac{\dot{m}_i}{\rho_e u_e b} \sqrt{\frac{u_e}{4\pi D_{12_e} x}} \quad .$$

Secondly, at a given value of the axial coordinate, the distribution of concentration across the wake is approximately Gaussian:

$$K/K_{\mathcal{L}} \cong e^{-u_e Y^2/4D_{12_e} x} \quad .$$

Experimental profiles of helium and argon concentration measured at $P_o = 10$ psig at fixed distances downstream of the model are plotted in Figures 19 and 20. These profiles show the approximately Gaussian distribution expected. Experimental values of maximum concentration along the centerline from 1.5 to 20 diameters downstream of the model are plotted in Figure 21. Downstream of the neck, these values show the expected behavior of $K_{\mathcal{L}} \sim x^{-\frac{1}{2}}$. By plotting $K^{-2}_{\mathcal{L}}$ versus x/d for both helium and argon injection, it appears that a "virtual" origin of laminar diffusion is located approximately one diameter downstream of the model (Figures 22 and 23).

Values of the binary diffusion coefficient, D_{12}, can be obtained from this data for comparison with theoretical predictions. In general, this process would involve tedious numerical procedures, but along the wake centerline the exact diffusion equation is considerably simplified because of wake symmetry. Along the centerline, the diffusion equation becomes:

$$\left(\rho u \frac{\partial K_i}{\partial x} \right)_{\mathcal{L}} = \left[\rho D_{12} \left(\frac{\partial^2 K_i}{\partial y^2} + \frac{M_1 M_2}{M^2} \frac{k_T}{T} \frac{\partial^2 T}{\partial y^2} \right) \right]_{\mathcal{L}} \quad ,$$

where $(\ldots)_{\mathcal{L}}$ indicates evaluation along the wake centerline. Solving

for $(D_{12})_{\mathfrak{L}}$:

$$(D_{12})_{\mathfrak{L}} = \left[\frac{u \frac{\partial K}{\partial x}}{\frac{\partial^2 K}{\partial y^2} + \frac{m_1 m_2}{m^2} \frac{k_T}{T} \frac{\partial^2 T}{\partial y^2}} \right]_{\mathfrak{L}} .$$

The quantity $(\partial K/\partial x)_{\mathfrak{L}}$ was evaluated from the experimental concentration data directly by taking the slope of $\ln(K_{\mathfrak{L}})$ plotted versus $\ln(x/d)$ (Figures 22 and 23) and using the relation

$$\left(\frac{\partial K}{\partial x} \right)_{\mathfrak{L}} = \left[\frac{K}{x} \frac{\partial \ln K}{\partial \ln (x/d)} \right]_{\mathfrak{L}} .$$

The quantity $u_{\mathfrak{L}}$ was determined from the equation:

$$u_{\mathfrak{L}} = (Ma)_{\mathfrak{L}} = (M \sqrt{\gamma RT})_{\mathfrak{L}} ,$$

where M, γ, R, and T were evaluated from concentration and pressure data by the method explained in Section III. 2.

The quantity $(\partial^2 K/\partial y^2)_{\mathfrak{L}}$ was determined from the experimental concentration profiles by assuming that near y = 0, the concentration profile shape could be approximated by:

$$K/K_{\mathfrak{L}} = e^{-(a_2 y^2 + a_4 y^4 + \ldots)} .$$

Then $(\partial^2 K/\partial y^2)_{\mathfrak{L}} = -2K_{\mathfrak{L}} a_2$.

If $\sqrt{\log_e (K_{\mathfrak{L}}/K)}$ is plotted versus y (Figures 24 and 25), $\sqrt{a_2}$ can be determined from the limiting slope near $y \longrightarrow 0$, because:

$$\sqrt{a_2} = \lim_{y \to 0} \left[\frac{\sqrt{\log_e (K_{\mathfrak{L}}/K)}}{y} \right] .$$

The quantity $(\partial^2 T/\partial y^2)_{\mathfrak{L}}$ is evaluated as a function of Mach number, reservoir temperature, static pressure, and total pressure, by utilizing symmetry of the wake about the centerline. If isoenergetic flow is assumed:

$$T = T_o / \left(1 + \frac{\gamma - 1}{2} M^2\right) \text{ where } T_o \text{ is constant, then}$$

$$\left(\frac{\partial^2 T}{\partial y^2}\right)_{\mathfrak{L}} = \left[\frac{-T^2}{T_o} (\gamma - 1) M \frac{\partial^2 M}{\partial y^2}\right]_{\mathfrak{L}} .$$

The Mach number is related to the pressure profile by the Rayleigh pitot equation:

$$\frac{p_{t_2}}{p_1} = \left[\frac{\gamma + 1}{2} M_1^2\right]^{\gamma/\gamma-1} \left[\frac{\gamma + 1}{2\gamma M_1^2 - (\gamma - 1)}\right]^{1/\gamma-1} ,$$

where p_1 is nearly constant across the inner wake. The equation for $\left(\frac{1}{T}\right)^2 T/\partial y^2)_{\mathfrak{L}}$ can finally be written:

$$\left(\frac{1}{T} \frac{\partial^2 T}{\partial y^2}\right)_{\mathfrak{L}} = \left[\frac{-T}{T_o} (\gamma - 1) \frac{M_1^2}{2 p_{t_2}} \frac{(2M_1^2 - \frac{\gamma - 1}{\gamma})}{(2 M_1^2 - 1)} \frac{\partial^2 p_{t_2}}{\partial y^2}\right]_{\mathfrak{L}} ,$$

where $\left(\frac{\partial^2 p_{t_2}}{\partial y^2}\right)_{\mathfrak{L}}$ is evaluated from the total pressure profiles.

In order to determine the effect of thermal diffusion, the value of k_T had to be found. Experimental determination of this parameter was not possible, but a theoretical formula for k_T is given by Hirschfelder, et al[4]:

$$k_T = \frac{N_1 N_2 \left[S^{(1)} N_1 - S^{(2)} N_2\right] (6 C_{12} - 5)}{6 \lambda_{12} (X_\lambda - Y_\lambda)} ,$$

where N_1 , N_2 = mole fractions of components 1 and 2, respectively, and $S^{(1)}$, $S^{(2)}$, λ_{12} , C_{12} , X_λ , Y_λ are functions of molecular weight, temperature, and intermolecular force constants tabulated by Hirschfelder.

A positive value of k_T signifies that component 1 tends to move into a cooler region, while a negative value signifies a tendency to move into a warmer region. At $0^\circ C$, for very small concentrations of tracer gas, $k_{T_{He}} \longrightarrow -0.25\, N_{He}$ and $k_{T_A} \longrightarrow +0.05\, N_A$. Changes in temperature will change the numerical value of k_T slightly, but the sign of k_T will remain the same. Since the wake center is warmer than the external flow, thermal diffusion will tend to slow down helium diffusion and speed up argon diffusion outward from the wake centerline.

From the experimental data, values of $T_{\mathfrak{C}}$, $M_{\mathfrak{C}}$, $\gamma_{\mathfrak{C}}$, $R_{\mathfrak{C}}$, $\left(\frac{1}{T}\frac{\partial^2 T}{\partial y^2}\right)_{\mathfrak{C}}$, $\left(\frac{\partial^2 K}{\partial y^2}\right)_{\mathfrak{C}}$, $\left(\frac{\partial K}{\partial x}\right)_{\mathfrak{C}}$, and $u_{\mathfrak{C}}$ were determined as described above. From these values the binary diffusion coefficients at the centerline, $(D_{12})_{\mathfrak{C}}$ were computed and are tabulated in Table 2. For purposes of comparison, the theoretical values of D_{12} were computed from an expression given by Hirschfelder, et al[4]:

$$D_{12} = \frac{0.002628}{P\,\sigma_{12}^2\,\Omega_{12}^{(1,1)}} \sqrt{\frac{T^3\,(\mathcal{M}_1 + \mathcal{M}_2)}{2\,\mathcal{M}_1\,\mathcal{M}_2}} \quad ,$$

where

P = pressure in atmospheres

T = temperature in degrees Kelvin

$\mathcal{M}_1, \mathcal{M}_2$ = molecular weights of components 1 and 2, respectively

$\Omega_{12}^{(1,1)}, \sigma_{12}$ = functions of temperature and intermolecular force constants tabulated by Hirschfelder.

This equation shows that for a binary mixture of two given gases, the quantity, $P D_{12}$, is a function of temperature alone. Values of $P D_{12}$ for helium-air mixtures and argon-air mixtures were calculated over a range of temperatures and are plotted in Figure 34, along with experimental values of $P D_{12}$. This plot shows good agreement between theoretical and experimental values.

The effect of thermal diffusion on the helium diffusion process was found to be approximately 20 to 30 per cent as large as the effect of molecular diffusion, and acted in an opposite direction, i. e., slowing diffusion outward from the center of the wake. The effect of thermal diffusion on argon diffusion was found to constitute less than 2 per cent of the total diffusion, and acted in the same direction as molecular diffusion.

III. 5. Diffusion of Mass in a Turbulent Wake

In a turbulent hypersonic wake, the mass diffusion processes are considerably complicated by the effect of random, rotational, three-dimensional vortices which greatly increase the rate of all diffusion processes. The description of mass diffusion in this type of flow by means of a simple equation does not appear to be feasible. Near the wake axis, however, there is good reason to believe that the transport of mass can be described in a semi-empirical manner by a relation of the form $\dot{m}_i = - \rho D_T (\partial K_i / \partial y)$, where D_T is a turbulent eddy diffusivity (See Townsend[16] for a discussion of the analogous momentum transfer process in a turbulent wake.). The turbulent diffusion equation near the wake axis is

$$\rho \bar{u} \frac{\partial K_i}{\partial x} + \rho \bar{v} \frac{\partial K_i}{\partial y} = \frac{\partial}{\partial y} \left(\rho D_T \frac{\partial K_i}{\partial y} \right) \quad ,$$

where $\bar{u}$ and $\bar{v}$ are mean velocity components at a point in the flow. In this equation, D_T encompasses all mass diffusion processes in the flow: turbulent eddy diffusion, molecular diffusion, etc.

In order to find a first order solution for K_i, we examine the flow far downstream of the model, and near the wake centerline. In this region we can assume that $\bar{u}$, ρ, and D_T are nearly constant and that $\bar{v}$ is zero. Then the diffusion equation takes the form:

$$\bar{u} \frac{\partial K_i}{\partial x} \cong D_T \frac{\partial^2 K_i}{\partial y^2} \quad .$$

The boundary conditions are identical to those for laminar flow:

(1) $y \longrightarrow \infty$, $K_i \longrightarrow 0$

(2) $$\int_{-\infty}^{\infty} \rho \bar{u} K_i \, dy = \text{constant} = \dot{m}_i / b \quad .$$

Therefore,

$$K_i \cong \frac{\dot{m}_i}{\rho \bar{u} b} \sqrt{\frac{\bar{u}}{4\pi D_T x}} \exp\left(-\bar{u} y^2 / 4 D_T x\right) \quad .$$

In the case of turbulent flow, it is expected that the concentration along the centerline will be approximately:

$$K_{\mathbb{C}} \cong \frac{\dot{m}_i}{\rho \bar{u} b} \sqrt{\frac{\bar{u}}{4\pi D_T x}} \sim x^{-\frac{1}{2}} \quad ,$$

and at a given value of the axial coordinate distribution of concentration across the wake will be approximately Gaussian:

$$\frac{K}{K_{\mathbb{C}}} \cong e^{-\bar{u} y^2 / 4 D_T x} \quad .$$

Experimental profiles of helium and argon concentration measured at P_o = 85 psig at fixed distances downstream of the model are plotted in Figures 26 and 27 and show the approximately Gaussian distribution expected. Experimental values of maximum concentration along the centerline from 2 to 30 diameters downstream of the model are plotted in Figures 28 and 29. Beyond ten diameters downstream of the model, these plots show the expected behavior of $K_{\mathfrak{C}} \sim x^{-\frac{1}{2}}$. But in regions of the flow closer to the model, the maximum concentration apparently decays more rapidly. This behavior is probably caused in part by the lower stream velocities in this region, relative to those downstream, which would permit a longer local "residence time" of the fluid, and a greater net transverse diffusion. By plotting $K_{\mathfrak{C}}^{-2}$ versus x/d for both helium and argon injection (Figures 30 and 31), it appears that a "virtual" origin of turbulent diffusion is located approximately 3.5 diameters downstream of the model. This virtual origin is where transition from laminar to turbulent flow appears to take place. Upstream of 3.5 diameters, the spreading rate is very slow, but downstream of this point, diffusion is much more rapid, indicating the probable onset of turbulence at this point.

In order to obtain specific values for the turbulent mass diffusion coefficient, D_T, from this data, the procedure of evaluating the diffusion equation at the centerline to take advantage of symmetry was again used. The expression for D_T, evaluated at the centerline is

$$(D_T)_{\mathfrak{C}} = \left[\frac{u \frac{\partial K}{\partial x}}{\frac{\partial^2 K}{\partial y^2}} \right]_{\mathfrak{C}}$$

Again, $(\partial^2 K/\partial y^2)_{\text{℄}}$ was evaluated by assuming that near y = 0, the concentration profile is of the form:

$$\frac{K}{K_{\text{℄}}} = e^{-(a_2 y^2 + a_4 y^4 + \ldots)} ,$$

so that $(\partial^2 K/\partial y^2)_{\text{℄}} = 2K_{\text{℄}} a_2$, where

$$a_2 = \lim_{y \to 0} \left[\frac{\log_e (K_{\text{℄}}/K)}{y^2} \right] .$$

Values for $\sqrt{a_2}$ were determined by plotting $\sqrt{\log_e (K_{\text{℄}}/K)}$ versus y (Figures 32 and 33) and evaluating the slope of the resulting lines near the origin.

Likewise, $\bar{u}_{\text{℄}}$ and $(\partial K/\partial x)_{\text{℄}}$ were evaluated from the concentration and pressure data in a manner identical to that outlined in the discussion of laminar flow (Section III. 4.). Values of $T_{\text{℄}}$, $M_{\text{℄}}$, $\gamma_{\text{℄}}$, $R_{\text{℄}}$, $(\partial^2 K/\partial y^2)_{\text{℄}}$, $(\partial K/\partial x)_{\text{℄}}$, and $\bar{u}_{\text{℄}}$ were determined in this way, and experimental values of D_T were calculated and tabulated in Table 2.

In order to compare the experimental values of D_T with the theoretical binary diffusion coefficient, D_{12}, the product of D_T and static pressure is plotted in Figure 34, along with P D_{12} values obtained earlier. The diffusion coefficients obtained at P_o = 85 psig are all considerably higher than the theoretical laminar values for the binary diffusion coefficients. In the case of helium diffusion, the values of D_T were about three times larger than the corresponding theoretical values for D_{12} . In the case of argon injection, this ratio was even greater, i. e., ten to one. This fact strongly indicates the presence of turbulence at this flow condition.

It has been suggested by Townsend[16], Mickelsen[9], and Saffman[14], that in certain cases the effects of turbulent eddy diffusion and molecular diffusion will be linearly additive, but data on this subject has been largely confined to subsonic, incompressible flow at pressures close to atmospheric. Near atmospheric pressure, the molecular diffusion coefficient, D_{12}, is very small relative to the turbulent diffusion coefficient, D_T. But D_{12} is inversely proportional to pressure, and at the very low static pressures of the flow in this investigation, the theoretical values for D_{12} in the case of helium were one-third the size of the measured turbulent diffusivity. Therefore, the effect of molecular diffusion in certain cases of turbulent diffusion may not be simply additive.

The mean values of D_T for the range of x/d in which measurements were made are $D_T = 0.11\ ft^2/sec^2$ for helium diffusion and $D_T = 0.14\ ft^2/sec^2$ for argon diffusion at $P_o = 85$ psig. Experimental values of D_T for given downstream distances are plotted in Figure 35. This plot shows that although there was considerable scatter, the average values of D_T changed very little with axial distances. Some estimates of the turbulent diffusivity, $\tilde{\varepsilon}_T$, for the turbulent diffusion of momentum have been made at GALCIT by L. Lees, using the equation:

$$\frac{\rho_e}{\rho_\infty} \frac{\tilde{\varepsilon}_T}{u_\infty d} \cong \frac{\tilde{K}}{4G_1} \left(\frac{C_{D_f}}{\beta} \right) ,$$

where

ρ_e is the density in the outer wake

ρ_∞ is the density ahead of the bow shock

G_1 is a profile shape parameter

$\beta = u_e/u_\infty$

$\tilde{K} = 0.06$ (K is inversely proportional to Townsend's[16] R_T)

The quantities ρ_e/ρ_∞ , u_∞ , $4G_1$, and β can be determined from pressure measurements made in the wake. C_{D_f} was estimated to be about 0.05. Using these values, it was found that

$$\tilde{\varepsilon}_T \cong 0.14 \text{ ft}^2/\text{sec}^2 \quad .$$

The quantity $\tilde{\varepsilon}_T$ cannot be considered to be equivalent to D_T , because one deals with the diffusion of momentum and the other with the diffusion of mass, but it was expected that they should be of the same order of magnitude. The close agreement found here between the two is probably coincidental, but it is more important to note that the experimental values for D_T were of the same order of magnitude as the predicted value of $\tilde{\varepsilon}_T$.

IV. CONCLUSIONS AND RECOMMENDATIONS FOR FUTURE WORK

1. The thermal conductivity method of gas analysis was shown to be a very satisfactory tool in the study of mass diffusion processes in hypersonic flow.

2. The injection of tracer gases was found to produce a measurable effect on the stagnation pressure in the wake. This effect was apparently caused by differences in molecular weight, enthalpy, and momentum between the injected gas and the gas in the free stream, and had to be allowed for in computations involving pressure.

3. The effect of probe tip dimensions on the experimental data should be investigated to determine whether the probe is drawing a true concentration sample of the gas in the wake and not smearing the shape of the profiles, especially in regions of large gradients of concentration.

4. The distribution of tracer gases in the hypersonic wake appeared to follow theoretical estimates of "similarity behavior" in both laminar and turbulent diffusion. Concentration profiles appeared Gaussian and the centerline concentration was approximately inversely proportional to the square root of the axial distance downstream.

5. At P_o = 10 psig (Re_d = 18,000) with a 0.3" circular cylinder, diffusion coefficients calculated from the experimental data, for both helium and argon diffusion in air, corresponded very closely to theoretical binary diffusion coefficients computed for laminar flow. It is reasonably certain that the inner wake at this flow condition was laminar as far downstream (15 diameters) as measurements could be made in this investigation.

6. At P_o = 85 psig, (Re_d = 72,000) diffusion coefficients calcu-

lated from the experimental data, for both helium and argon diffusion in air, were consistently much higher than theoretical diffusion coefficients for laminar flow at the same pressure and temperature. This greatly accelerated mixing process is ascribed to the presence of turbulence in the inner wake.

7. The effect of thermal gradients cannot be neglected when considering laminar mass diffusion processes in a hypersonic wake, especially in the diffusion of light gases. In the specific example in this investigation of helium diffusion in a laminar wake, the thermal diffusion effect was found to account for up to 30 per cent of the net mass diffusion.

8. In the turbulent diffusion of a tracer gas with low molecular weight, the mass diffusion rate attributed to molecular diffusion may be expected to be of the same order of magnitude as that caused by turbulent diffusion. Further investigation into this borderline area might produce valuable information regarding the relationship between the two processes.

9. The diffusion of very heavy gases, such as krypton or xenon, can be expected to show a very strong contrast between laminar and turbulent diffusion rates. Investigation of the diffusion of these gases would be especially valuable in a region of transition from laminar to turbulent flow.

10. More information about diffusion processes in a hypersonic wake can be obtained if a cylindrical model of smaller diameter is utilized. This smaller cylinder would enable measurements to be made much further downstream in terms of model diameters and might reveal the nature of the interaction of the inner wake and the "outer wake" generated by the bow shock wave.

REFERENCES

1. Ames Research Staff: Equations, Tables and Charts for Compressible Flow, NACA TR 1135, Ames Aeronautical Research Laboratory, 1953.

2. Daynes, H. A.: Gas Analysis by Measurement of Thermal Conductivity, Cambridge University Press, 1933.

3. Goldstein, S.: Modern Developments in Fluid Dynamics, Vol. II, Oxford University Press, 1938.

4. Hirschfelder, J. O.; C. F. Curtiss; and R. B. Bird: Molecular Theory of Gases and Liquids, John Wiley and Sons, New York, 1954.

5. Jeans, J.: Kinetic Theory of Gases, Cambridge University Press, 1946.

6. Kennard, E. H.: Kinetic Theory of Gases, McGraw-Hill Book Co., New York, 1938.

7. Liepmann, H. W. and A. Roshko: Elements of Gas Dynamics, John Wiley and Sons, New York, 1957.

8. Massey, H. S. W. and E. H. S. Burhop: Electronic and Ionic Impact Phenomena, Clarendon Press, Oxford, 1952.

9. Mickelson, W. R.: "Measurements of the Effect of Molecular Diffusivity in Turbulent Diffusion", Journal of Fluid Mechanics, Vol 7, Part 3, p. 397, Cambridge University Press, March, 1960.

10. Mohlenhoff, W.: Experimental Study of Helium Diffusion in the Wake of a Circular Cylinder at M = 5.8, GALCIT Hypersonic Research Project, Memorandum No. 54, May 20, 1960.

11. Pai, S. I.: Fluid Dynamics of Jets, D. Van Nostrand Co., New York, 1954.

12. Prandtl, L.: The Mechanics of Viscous Fluids, Durand: Aerodynamic Theory, Vol. III, Guggenheim Aeronautical Laboratory, 1934.

13. Rush, D. and W. Forstall, Jr.: Apparatus for the Determination of the Concentration of Helium in Air by the Thermal Conductivity Method, M. I. T. Internal Report No. 4 for Project Meteor, M. I. T., 1947.

14. Saffman, P. G.: "On the Effect of Molecular Diffusivity in Turbulent Diffusion", Journal of Fluid Mechanics, Vol. 8, Part 2, p. 273, Cambridge University Press, June, 1960.

15. Schlichting, H.: Boundary Layer Theory, McGraw-Hill Book Co., New York, 1960.

16. Townsend, A. A.: The Structure of Turbulent Shear Flow, Cambridge University Press, 1956.

TABLE 1

SELECTED GAS PROPERTIES

(1)	(2)	(3)	(4)	(5)
Gas	Chemical Formula	Molecular Weight	Ratio of Conductivity to Air at $0^{\circ}C$	D_{12} in Air at 1 atm, and $0^{\circ}C$
Air	--	28.952	1	--
Argon	A	39.944	0.684	0.158
Carbon Dioxide	CO_2	44.01	0.605	0.113
Helium	He	4.003	5.97	0.74
Hydrogen	H_2	2.0156	7.15	0.73
Krypton	Kr	83.7	0.360	0.113
Methane	CH_4	16.03	1.25	0.172
Neon	Ne	20.183	1.93	0.30
Nitrogen	N_2	28.016	0.996	0.175
Oxygen	O_2	32.000	1.013	0.171
Water Vapor	H_2O	18.02	0.775	--
Xenon	X	131.3	0.210	0.089

Column References:

(2), (3) Handbook of Chemistry and Physics, 31st edition, Chemical Rubber Publishing Co., 1949.

(4) Daynes, H. A., Gas Analysis by Measurement of Thermal Conductivity, Cambridge University Press, 1933.

(5) Hirschfelder, J. O. et al, Molecular Theory of Gases and Liquids, John Wiley and Sons, 1954.

TABLE 2

SUMMARY OF DIFFUSION COEFFICIENTS

CALCULATED FROM EXPERIMENTAL DATA

P_o(psig)	Tracer Gas	x/d	* D_K (ft^2/sec)
10	Helium	5	0.251
10	Helium	7	0.216
10	Helium	9	0.218
10	Helium	12	0.285
10	Helium	15	0.261
10	Argon	5	0.0555
10	Argon	7	0.0595
10	Argon	9	0.0587
10	Argon	12	0.0640
10	Argon	15	0.0638
85	Helium	5	0.118
85	Helium	7	0.1245
85	Helium	9	0.1028
85	Helium	12	0.1237
85	Helium	15	0.1185
85	Helium	19	0.116
85	Helium	24	0.096
85	Argon	5	0.160
85	Argon	7	0.1355
85	Argon	9	0.156
85	Argon	12	0.134
85	Argon	15	0.152
85	Argon	19	0.130
85	Argon	24	0.146

* At P_o = 10 psig; $D_K = K_{12}$ (laminar)

At P_o = 85 psig; $D_K = D_T$ (turbulent)

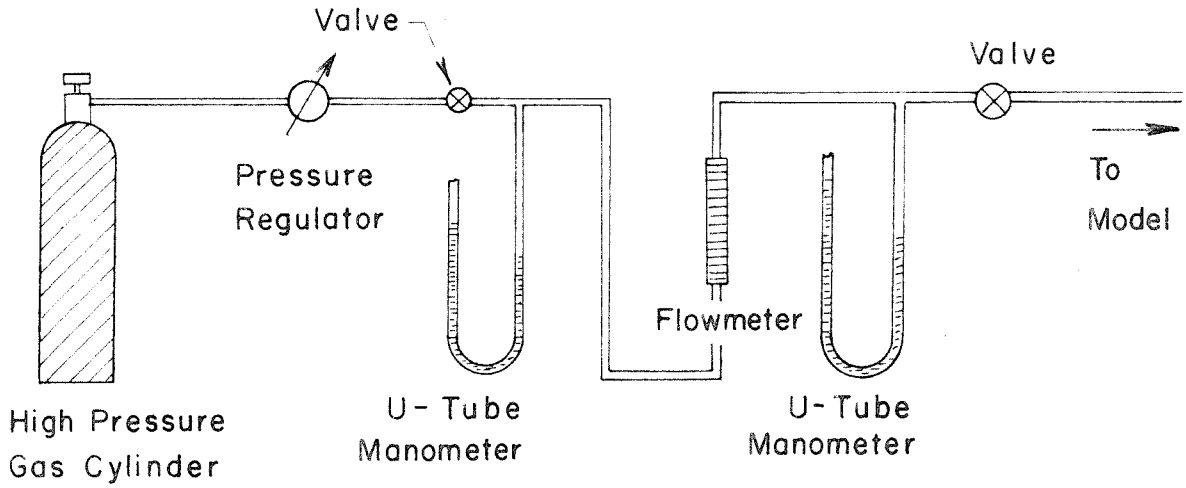

FIG. 1 - DIAGRAM OF INJECTION GAS SUPPLY

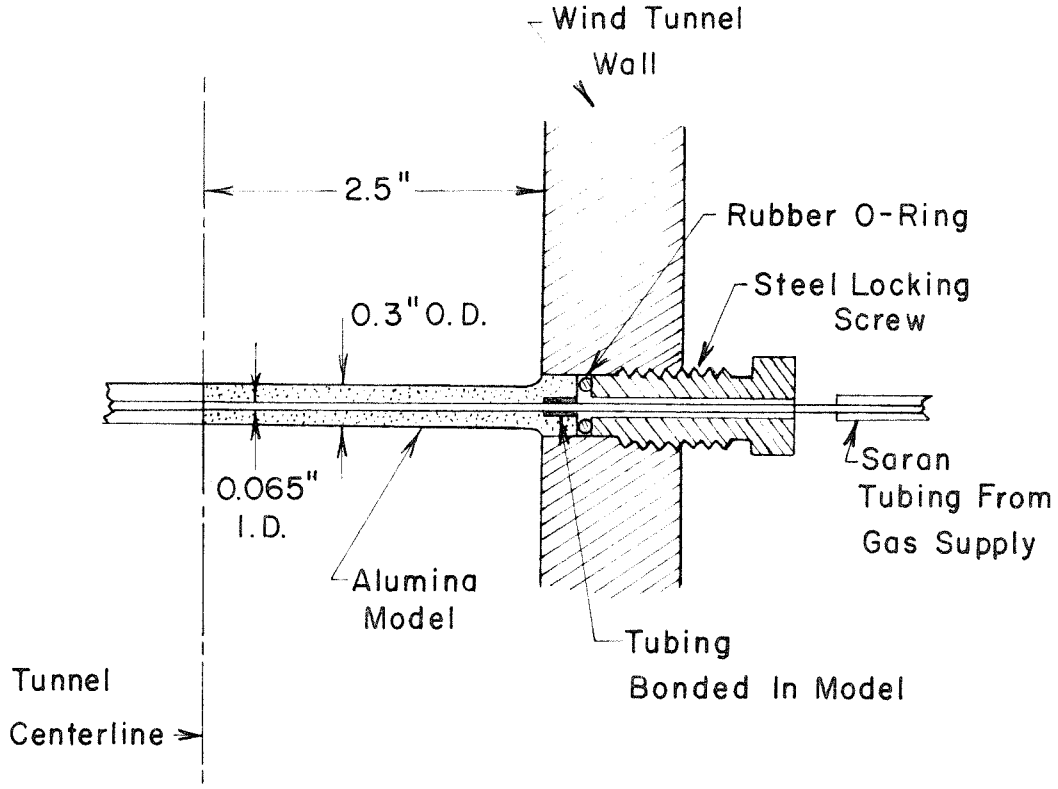

FIG. 2 - CROSS-SECTION VIEW OF MODEL INSTALLATION

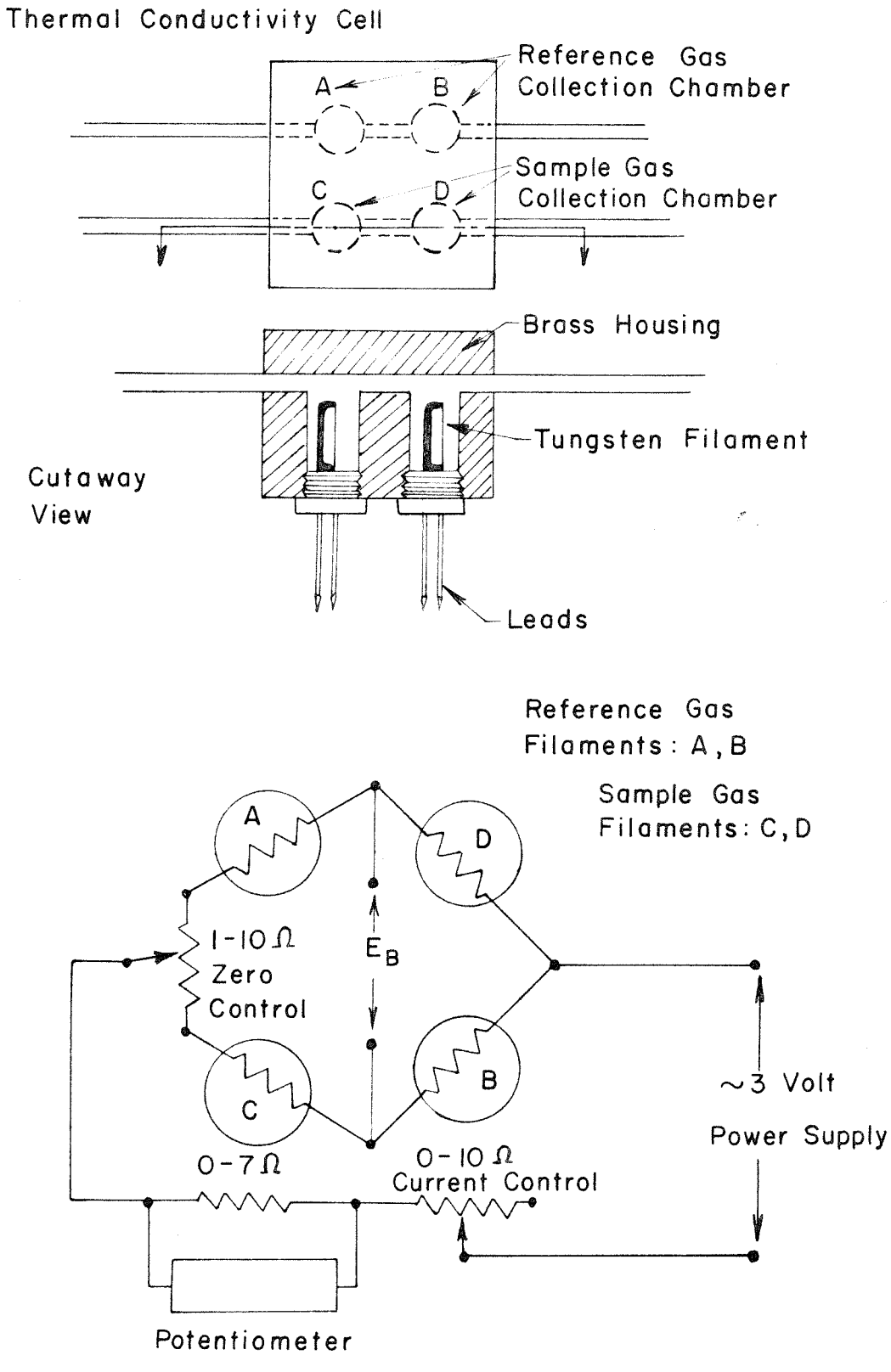

FIG. 3 - THERMAL CONDUCTIVITY CELL GEOMETRY AND WIRING DIAGRAM

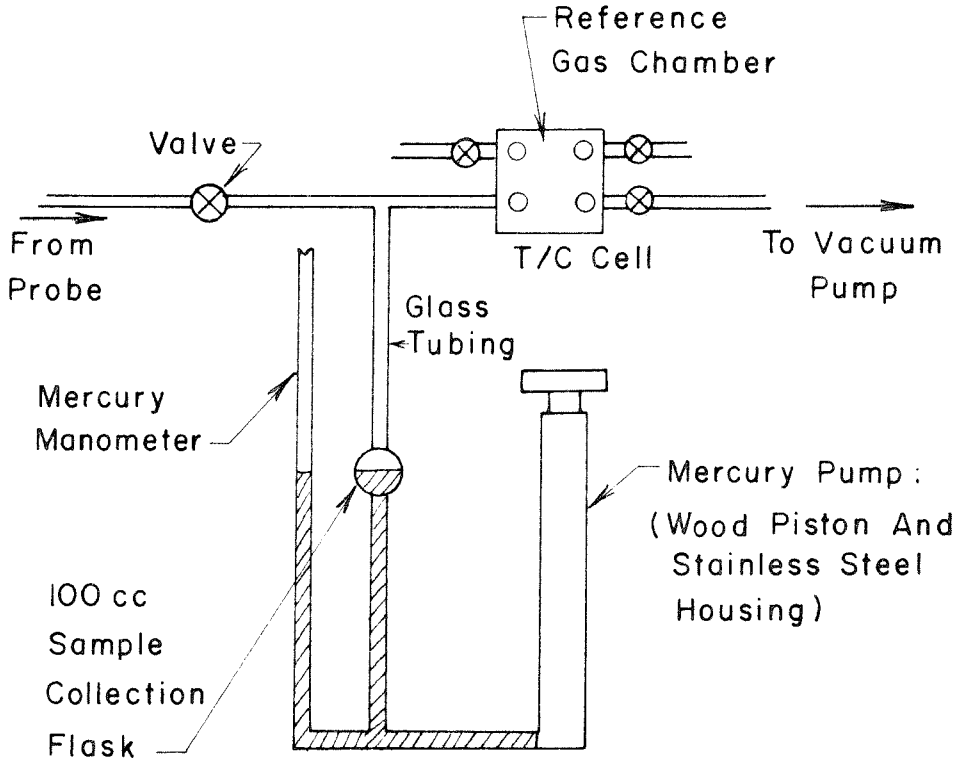

FIG. 4 - DIAGRAM OF SAMPLE GAS COLLECTION APPARATUS

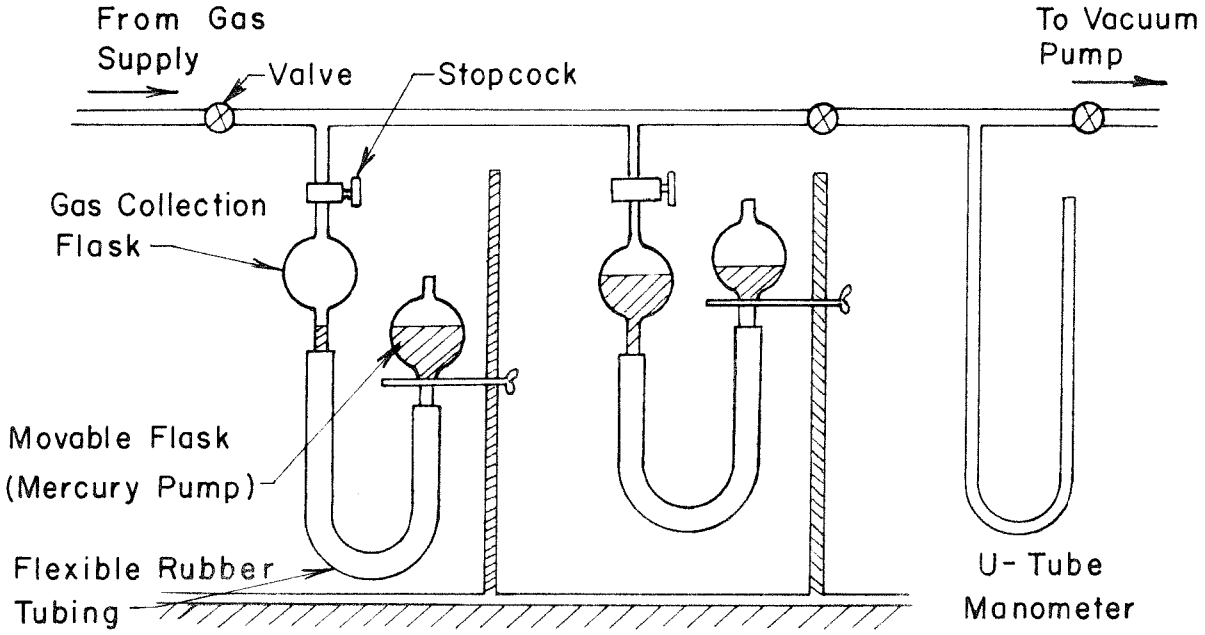

FIG. 5 – DIAGRAM OF APPARATUS USED TO MIX GAS SAMPLES FOR CELL CALIBRATION

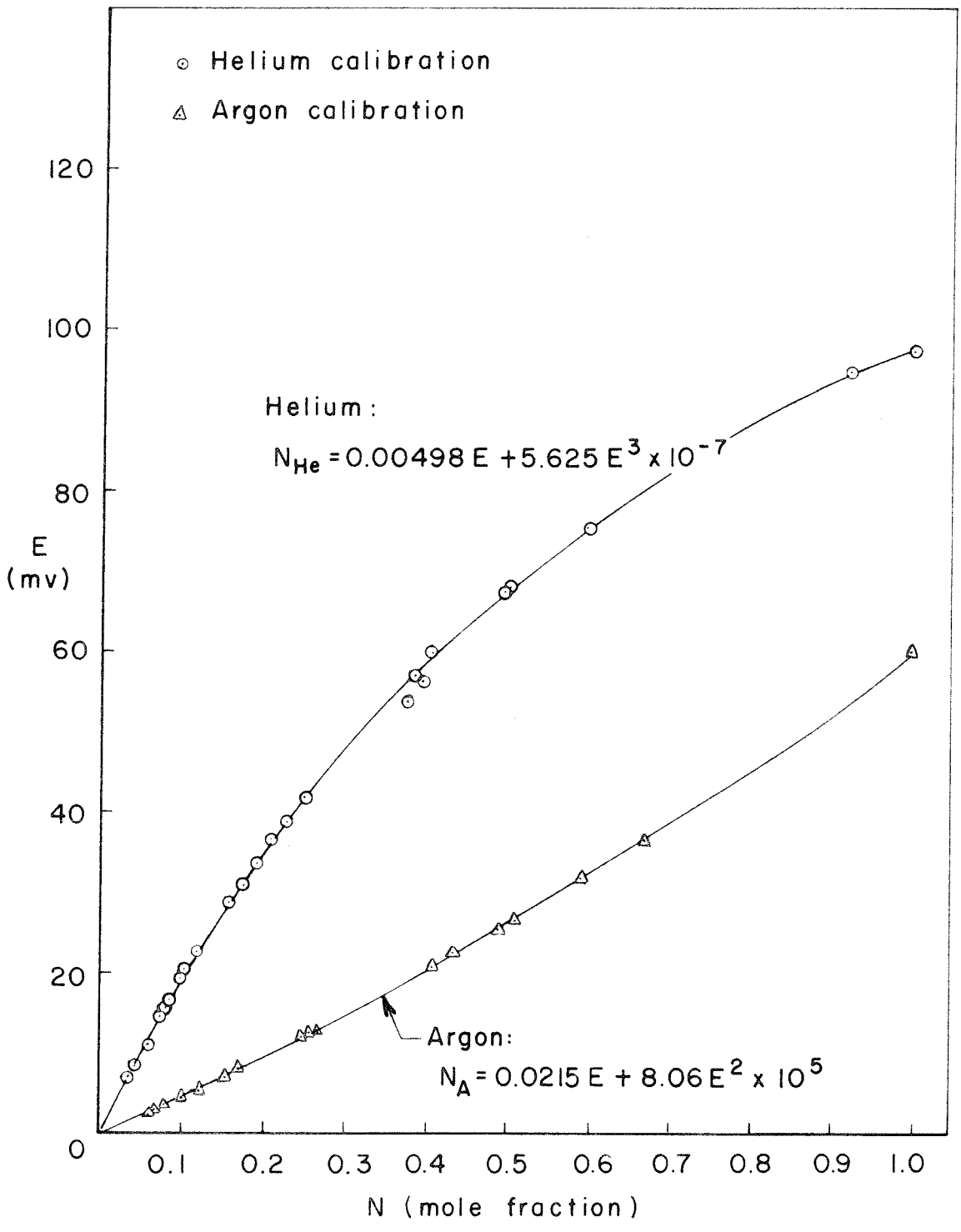

FIG. 6 - BRIDGE VOLTAGE CALIBRATION FOR HELIUM AND ARGON IN DRY AIR AT ATMOSPHERIC PRESSURE

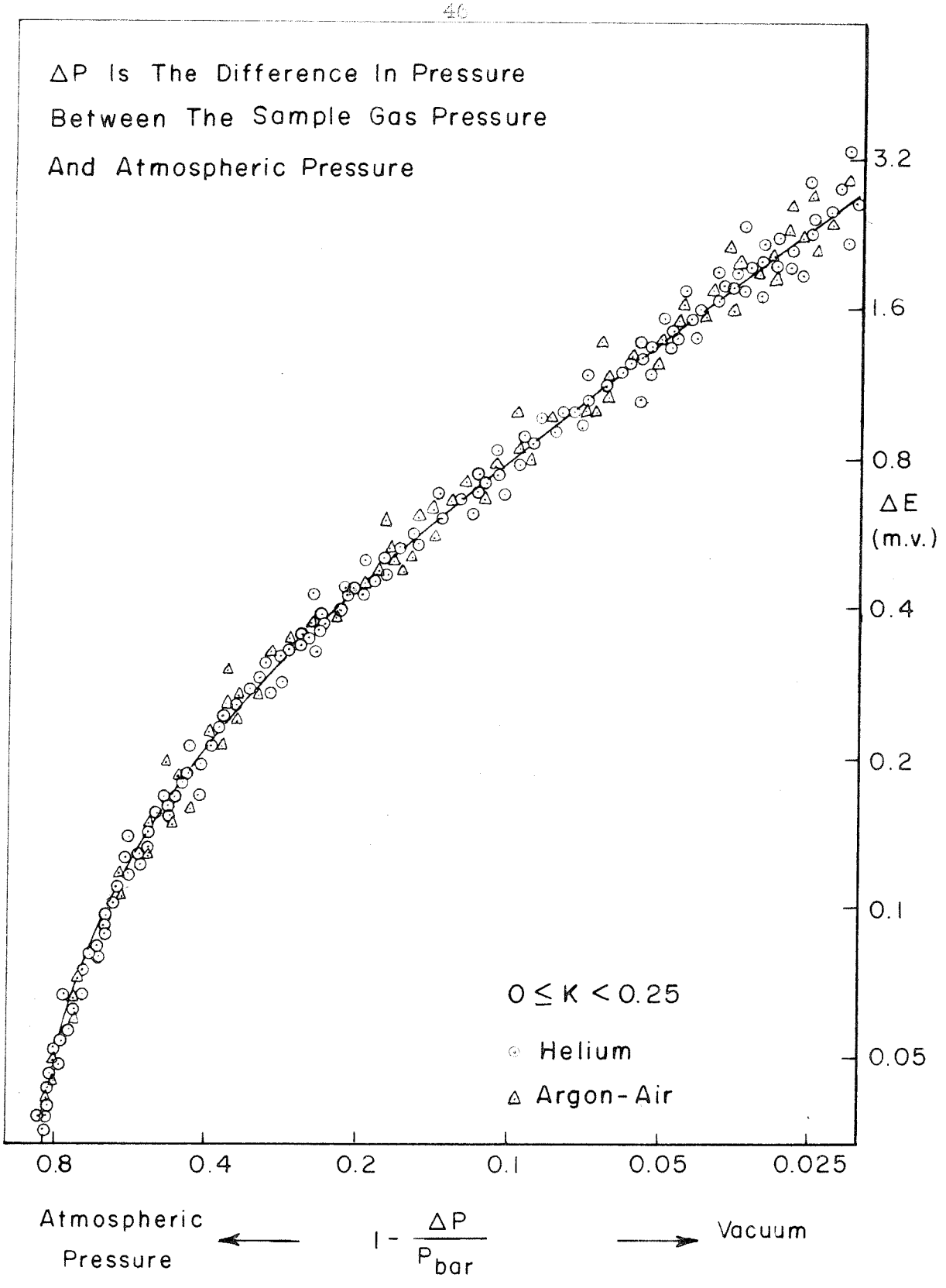

FIG. 7 - VOLTAGE CORRECTION FOR LOW SAMPLE GAS PRESSURES

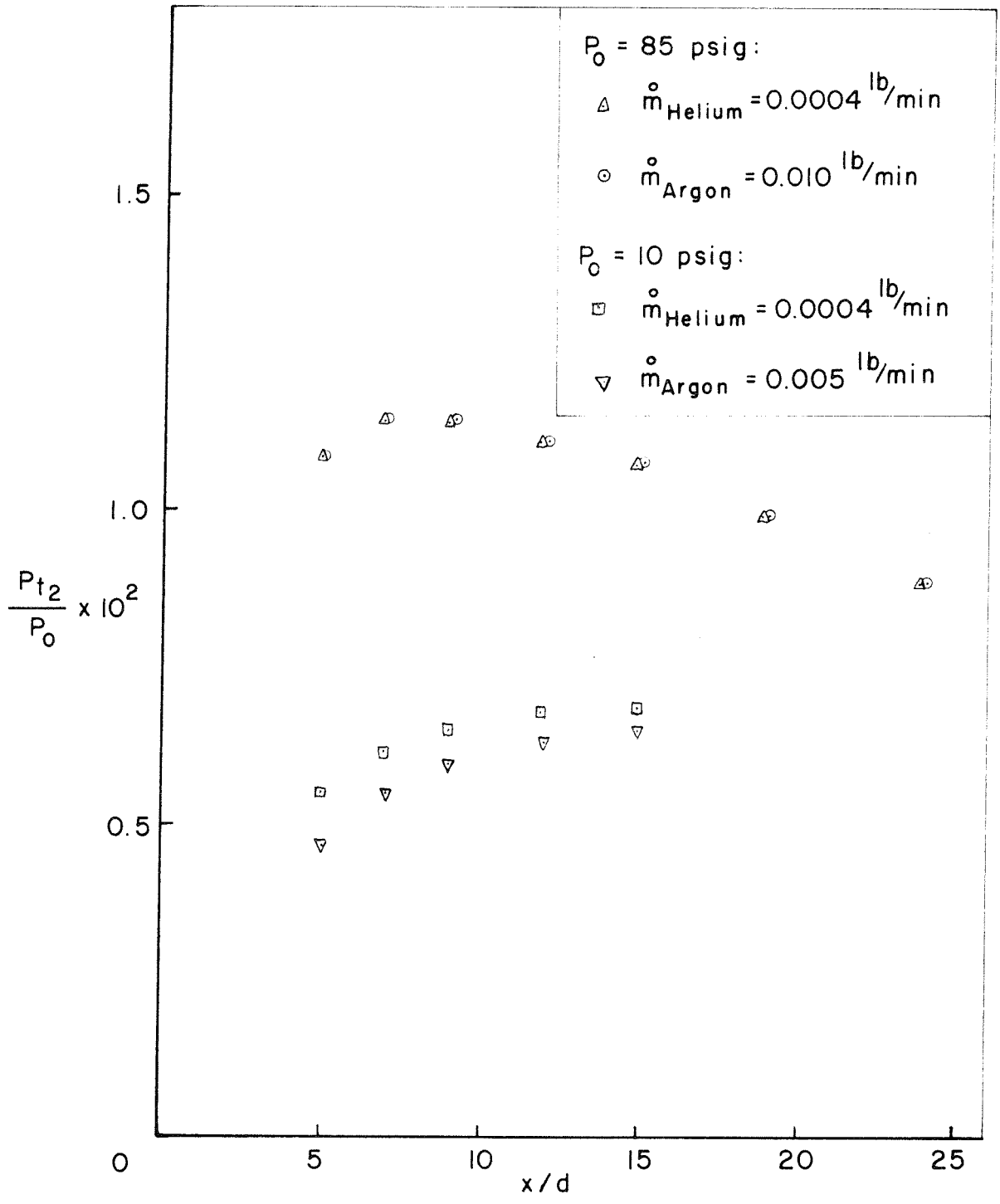

FIG. 8 - EXPERIMENTAL PROBE STAGNATION PRESSURES ALONG THE WAKE CENTERLINE

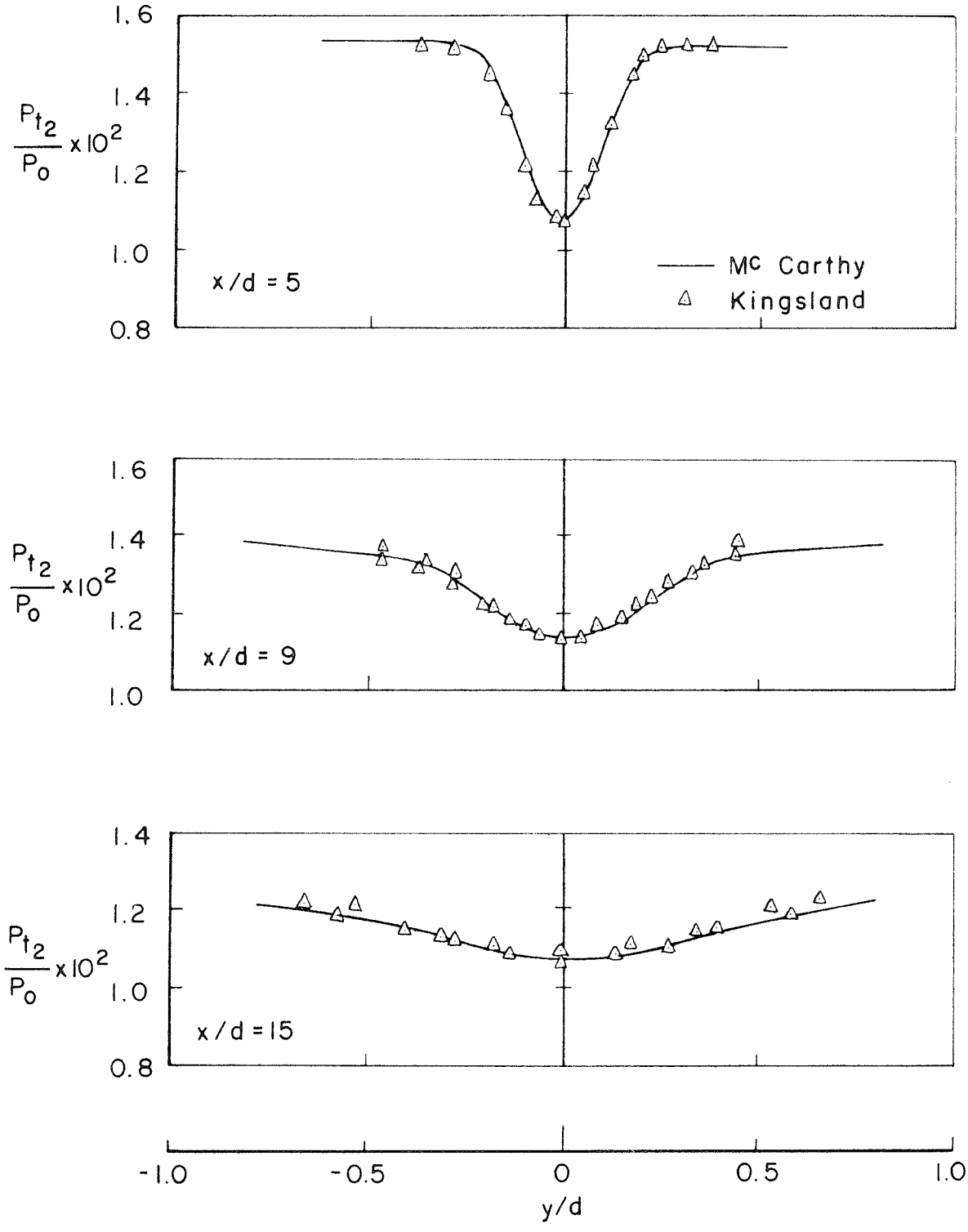

FIG. 9 – COMPARATIVE EXPERIMENTAL PROBE STAGNATION PRESSURE PROFILES AT P_o = 85 PSIG

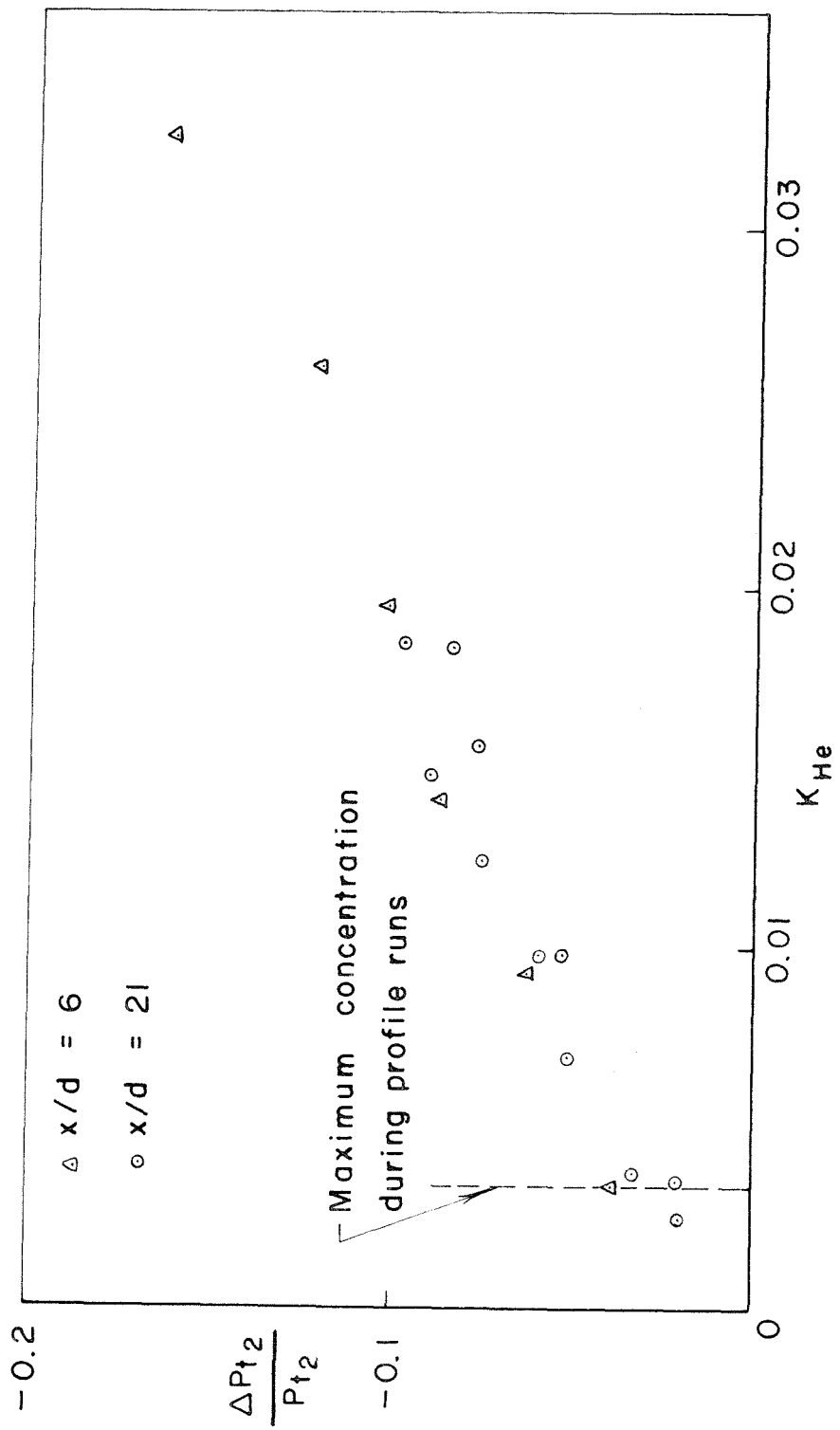

FIG. 10 - EFFECT OF HELIUM INJECTION ON PROBE STAGNATION PRESSURE AT P_o = 10 PSIG

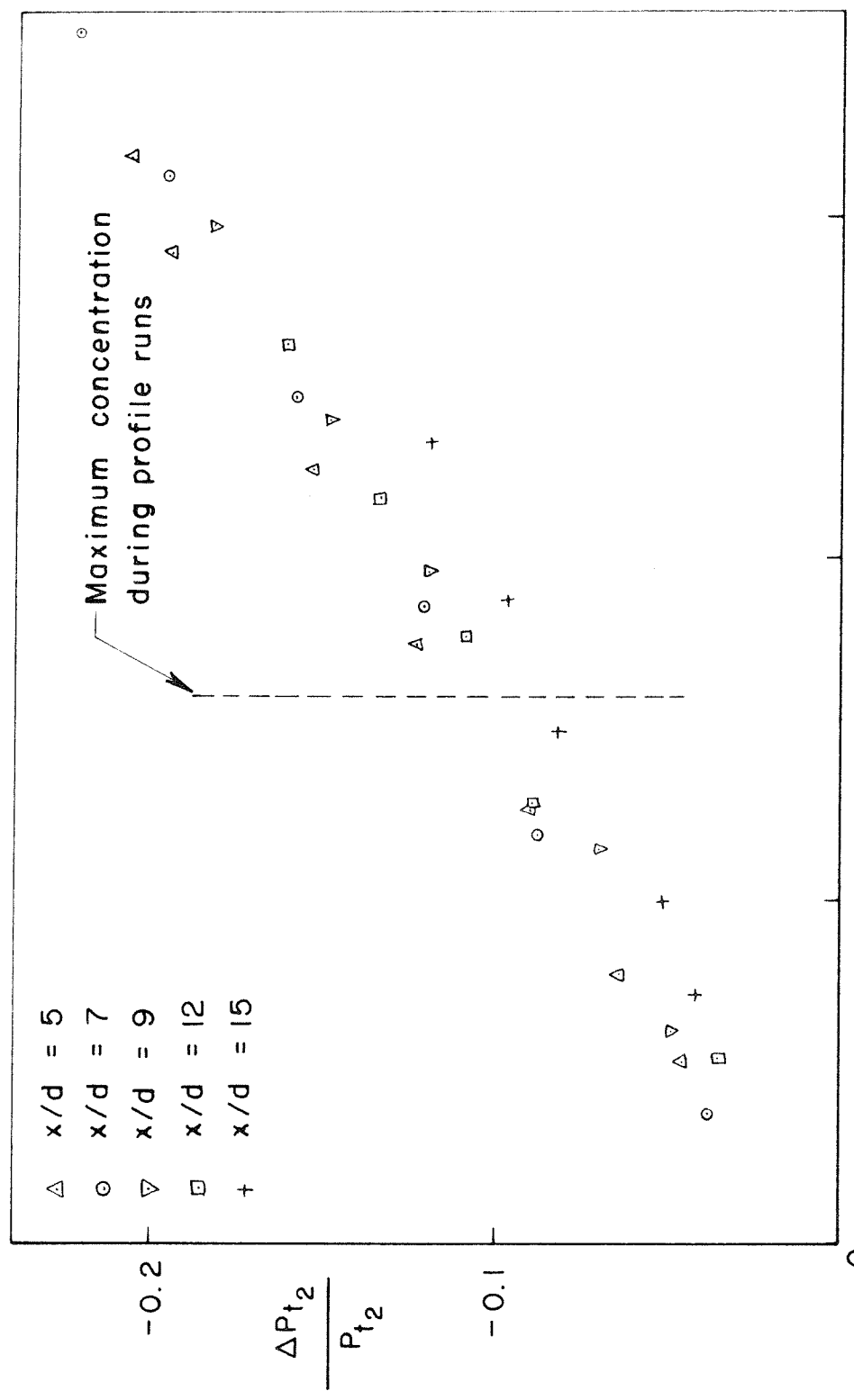

FIG. 11 – EFFECT OF ARGON INJECTION ON PROBE STAGNATION PRESSURE AT P_o = 10 PSIG

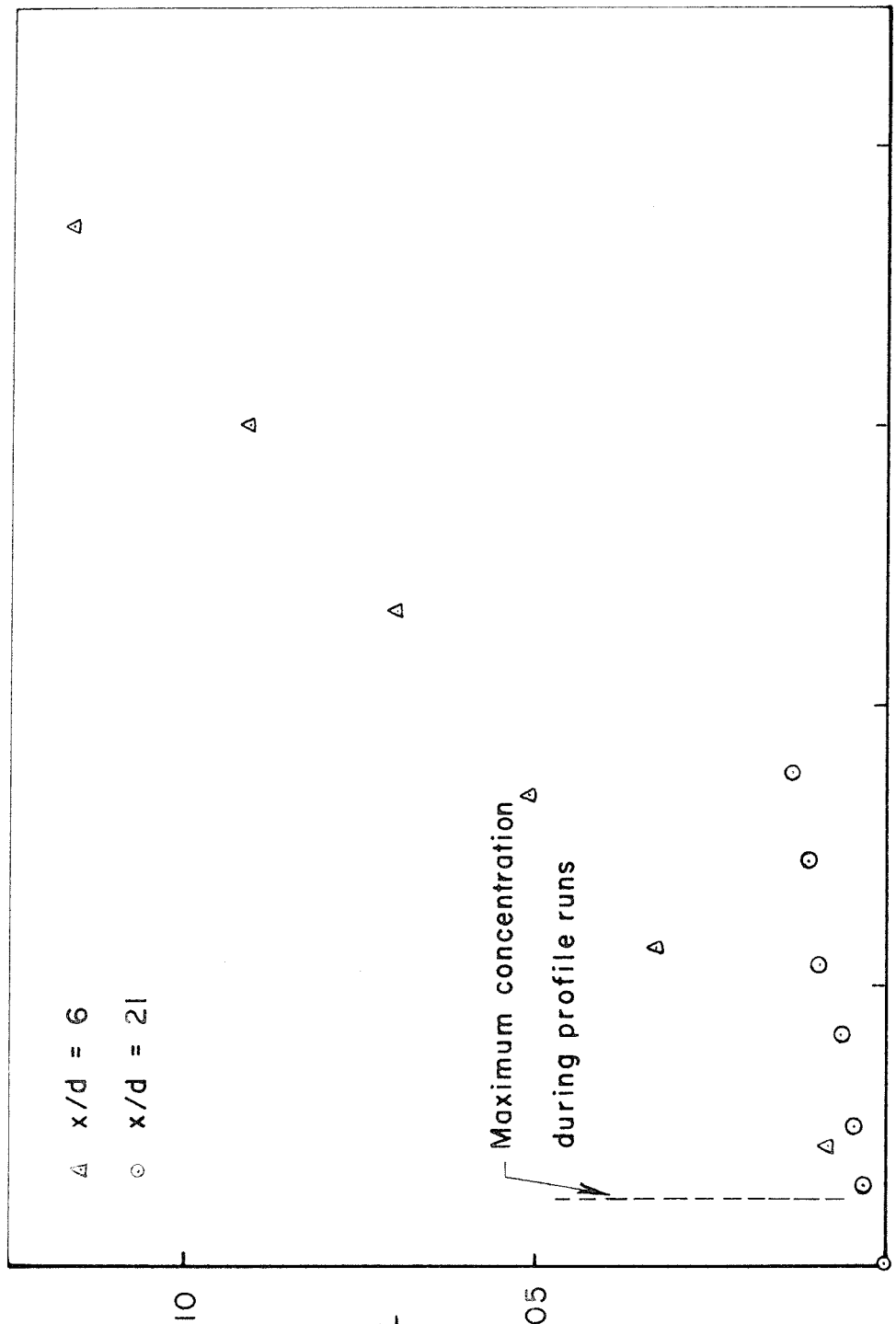

FIG. 12 - EFFECT OF HELIUM INJECTION ON PROBE STAGNATION PRESSURE AT P_o = 85 PSIG

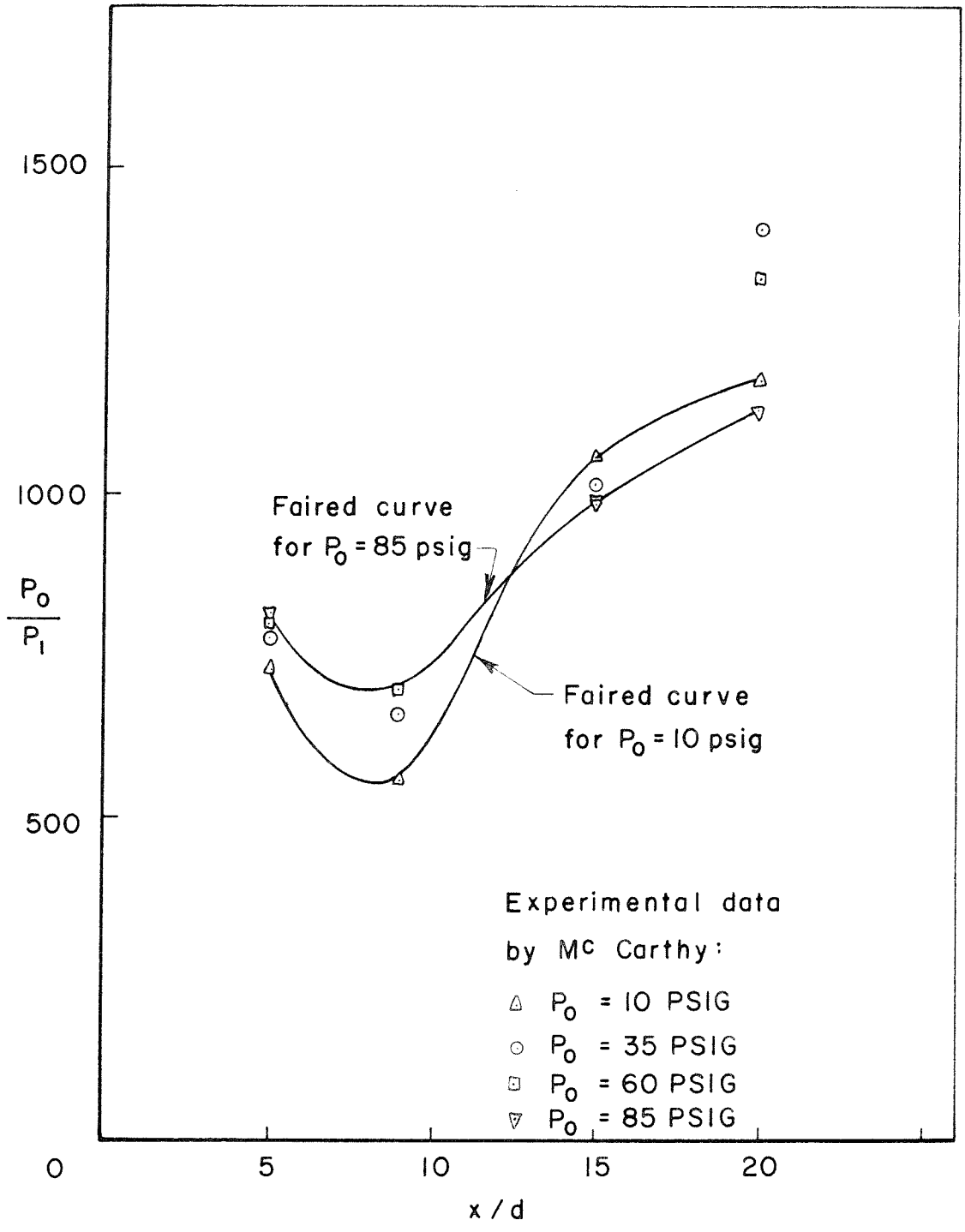

FIG. 13 - STATIC PRESSURE ALONG THE WAKE CENTERLINE

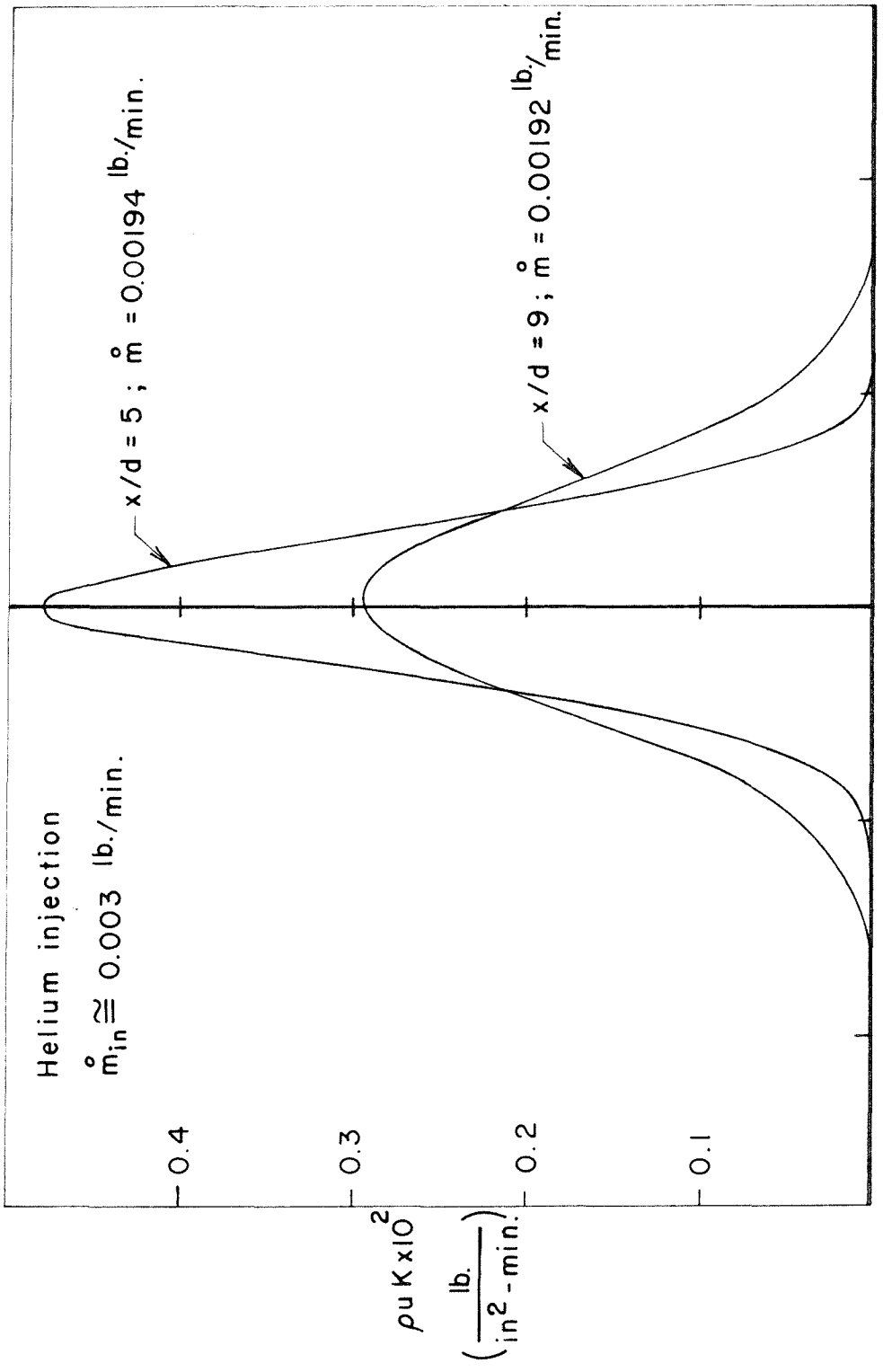

FIG. 14 - CONTINUITY PROFILES FOR HELIUM INJECTION AT P_o = 85 PSIG
(27 DEC. '60)

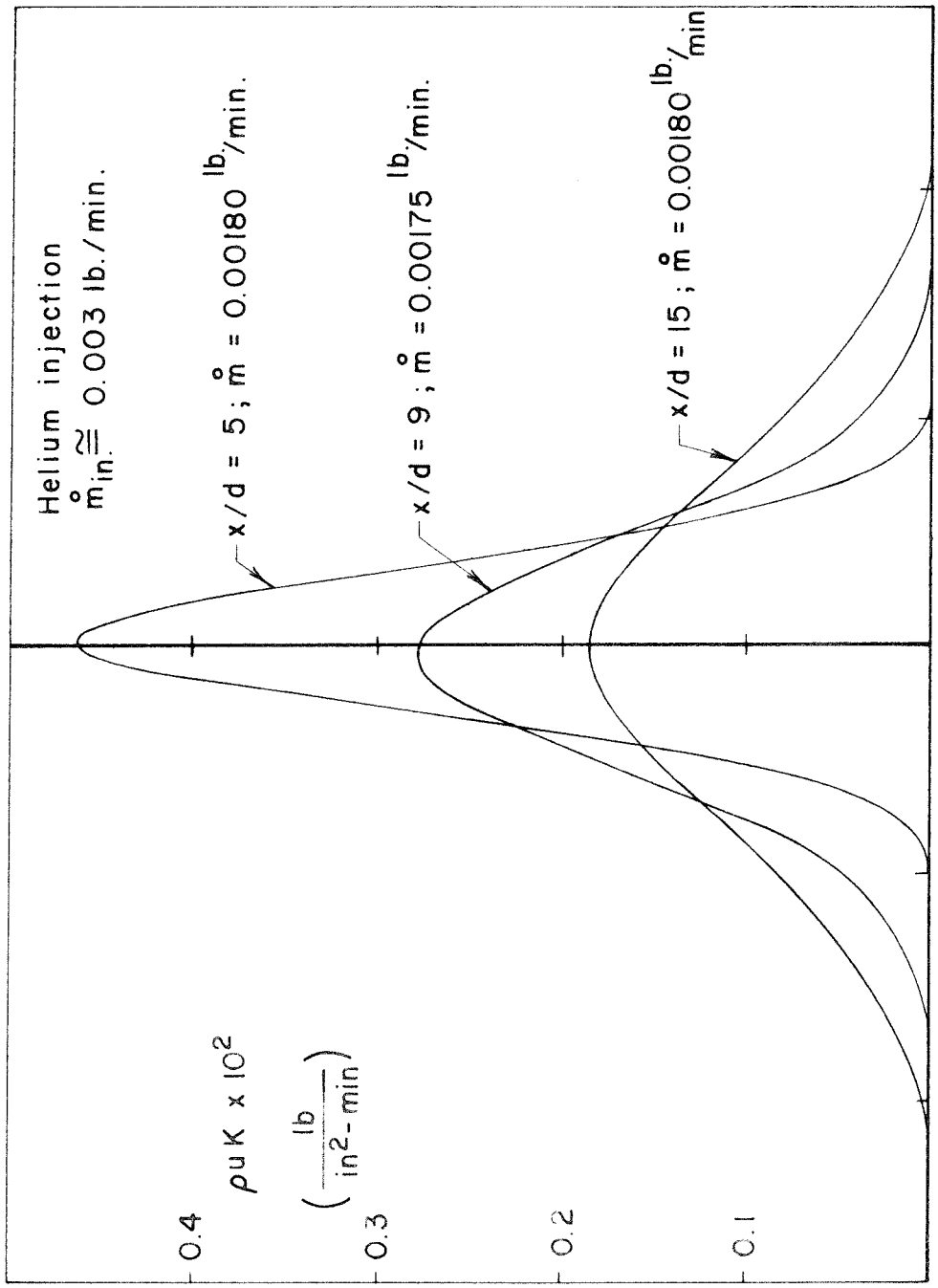

FIG. 15 - CONTINUITY PROFILES FOR HELIUM INJECTION AT P_o = 85 PSIG (5 JAN '61)

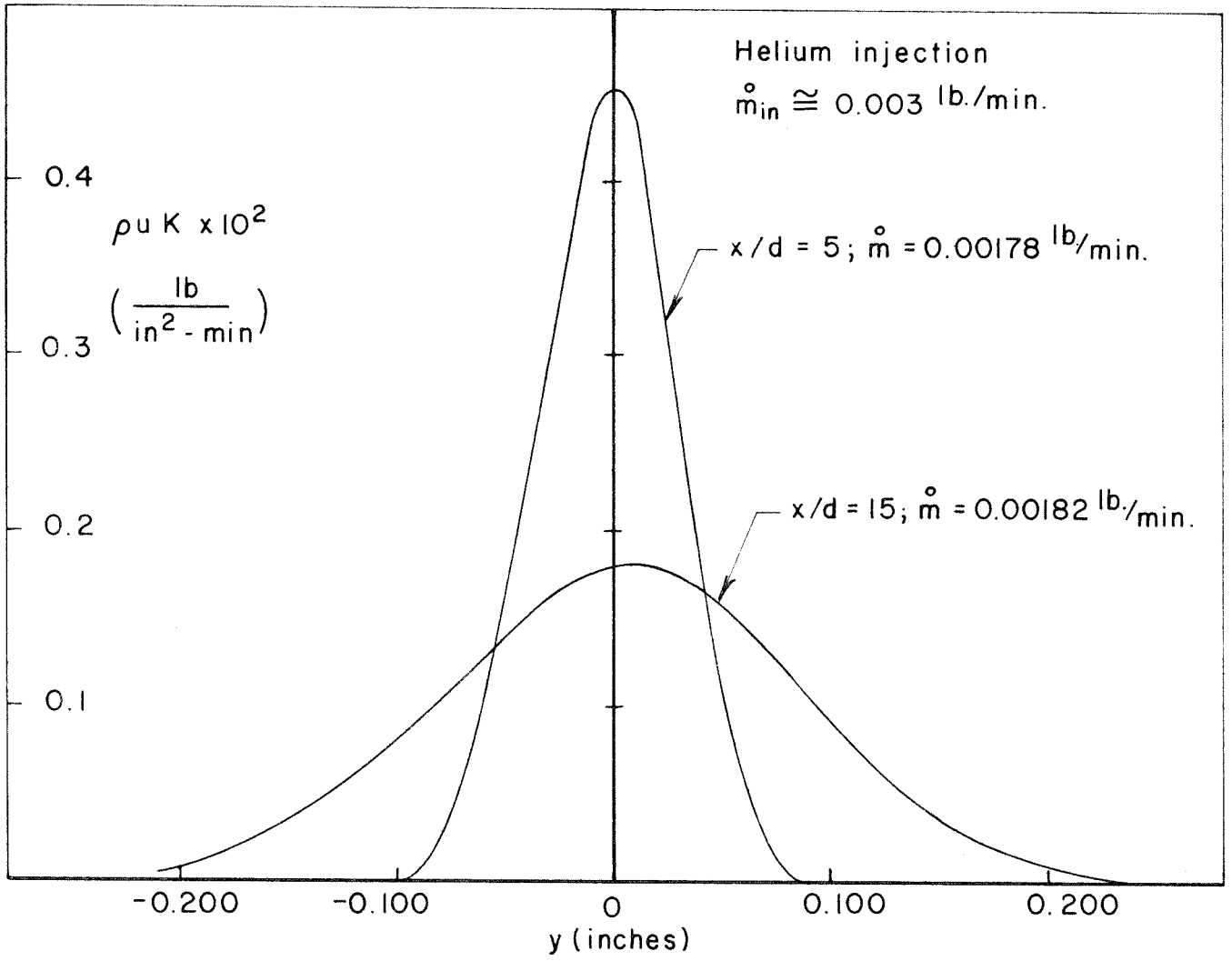

FIG. 16 - CONTINUITY PROFILES FOR HELIUM INJECTION AT P_0 = 85 PSIG (17 JAN '61)

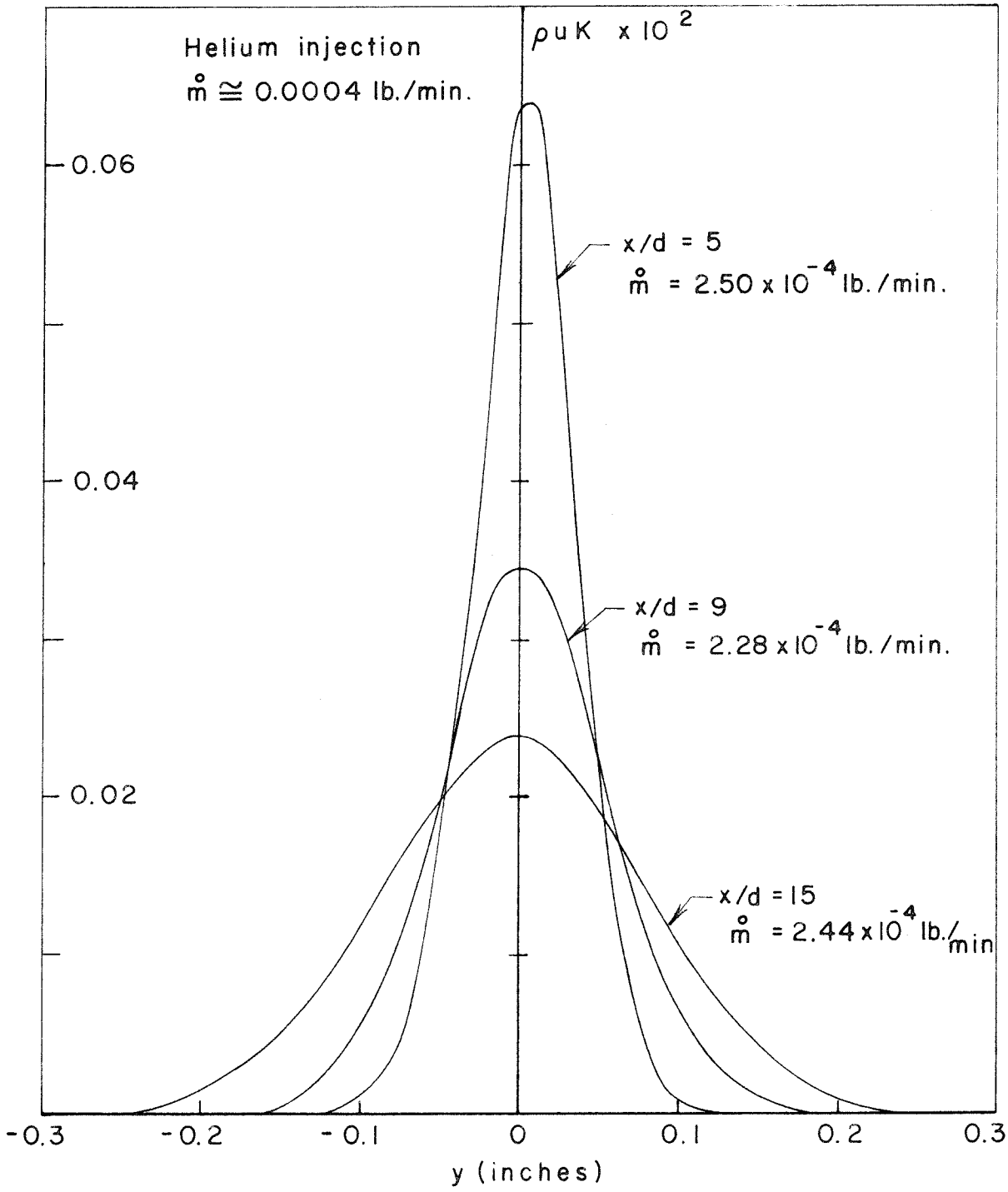

FIG. 17 - CONTINUITY PROFILES FOR HELIUM INJECTION AT P_o = 85 PSIG (FINAL TEST DATA)

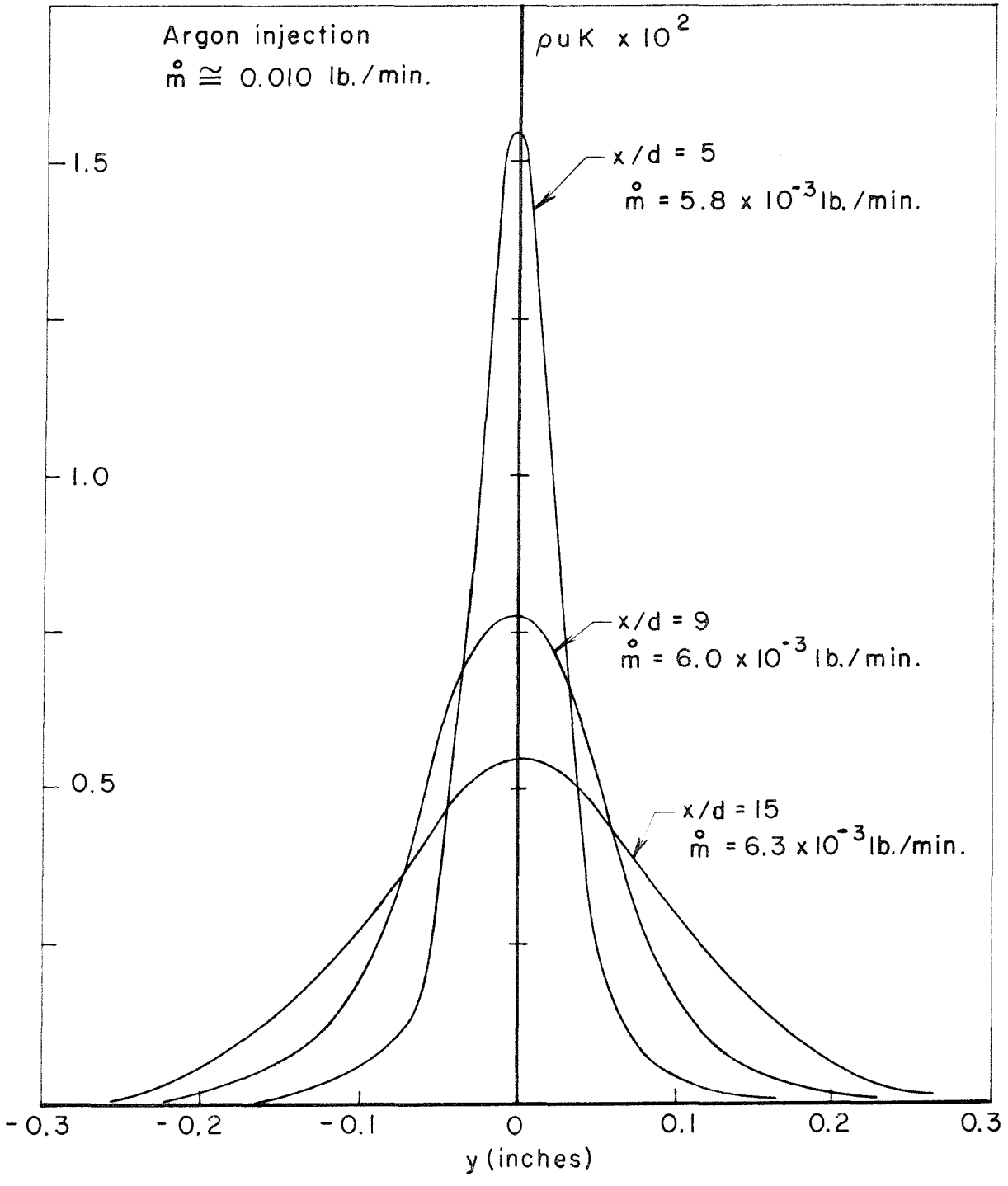

FIG. 18 - CONTINUITY PROFILES FOR ARGON INJECTION AT P_o = 85 PSIG (FINAL TEST DATA)

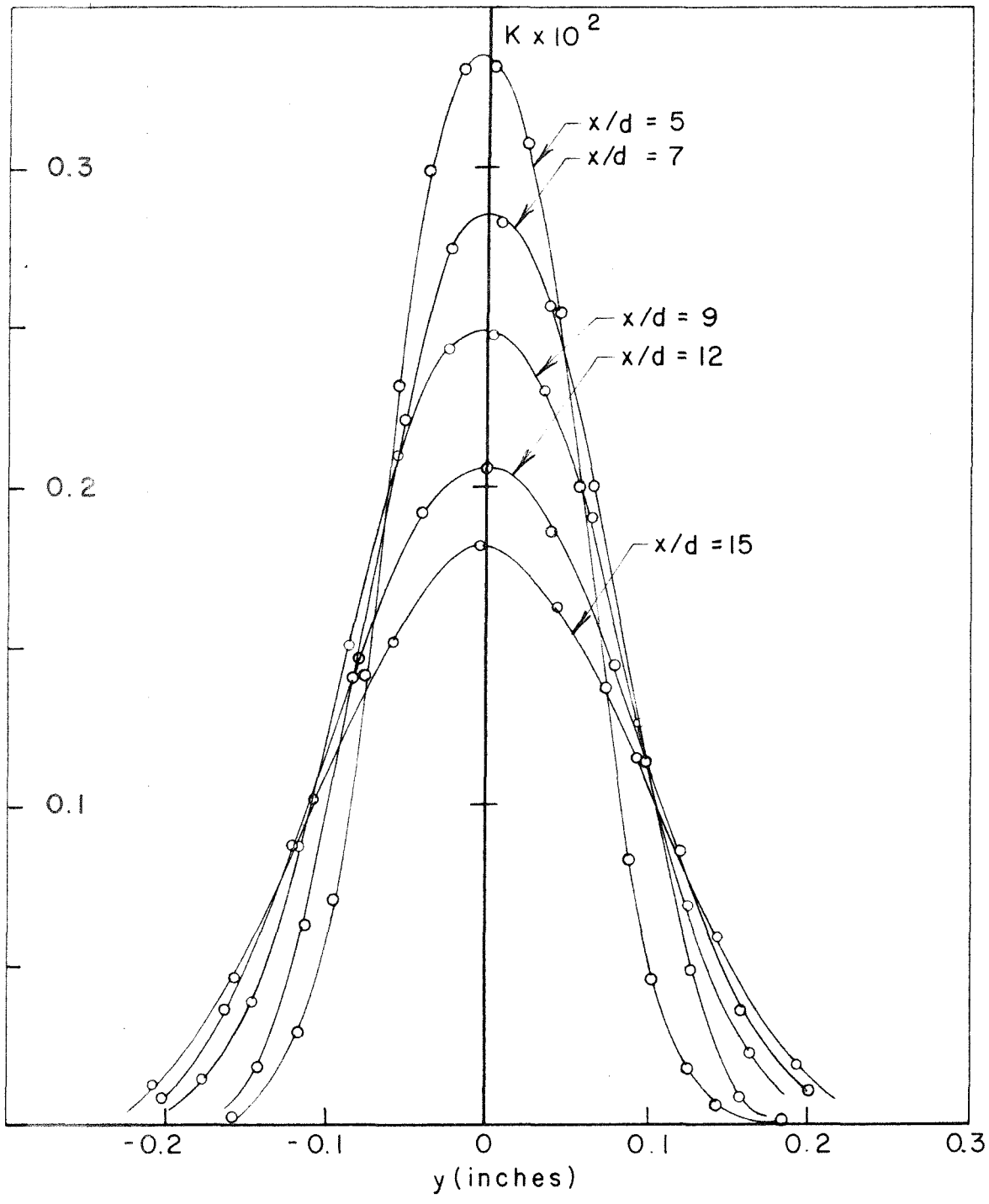

FIG. 19 - HELIUM MASS FRACTION PROFILES AT P_0 = 10 PSIG

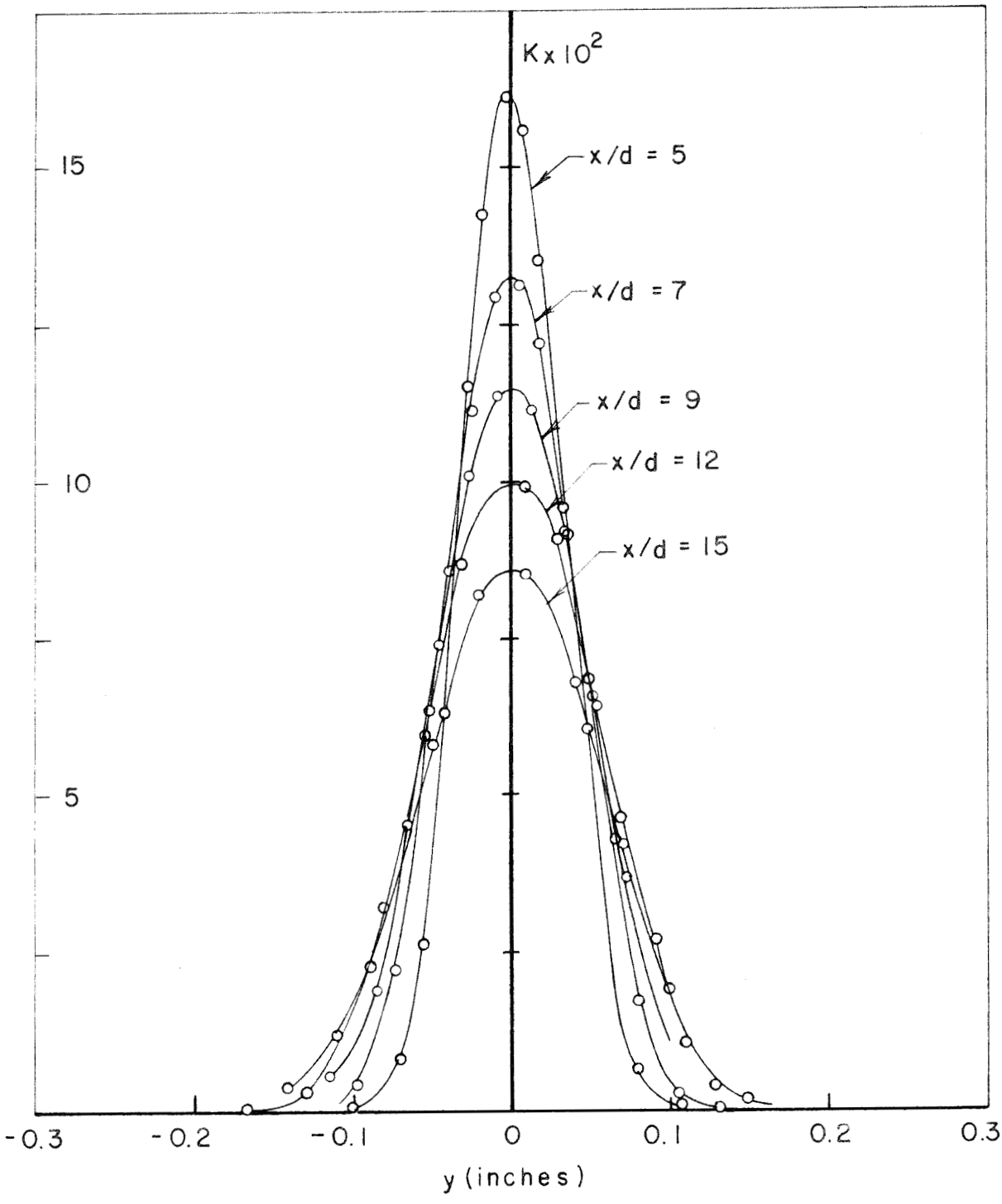

FIG. 20 - ARGON MASS FRACTION PROFILES AT P_0 = 10 PSIG

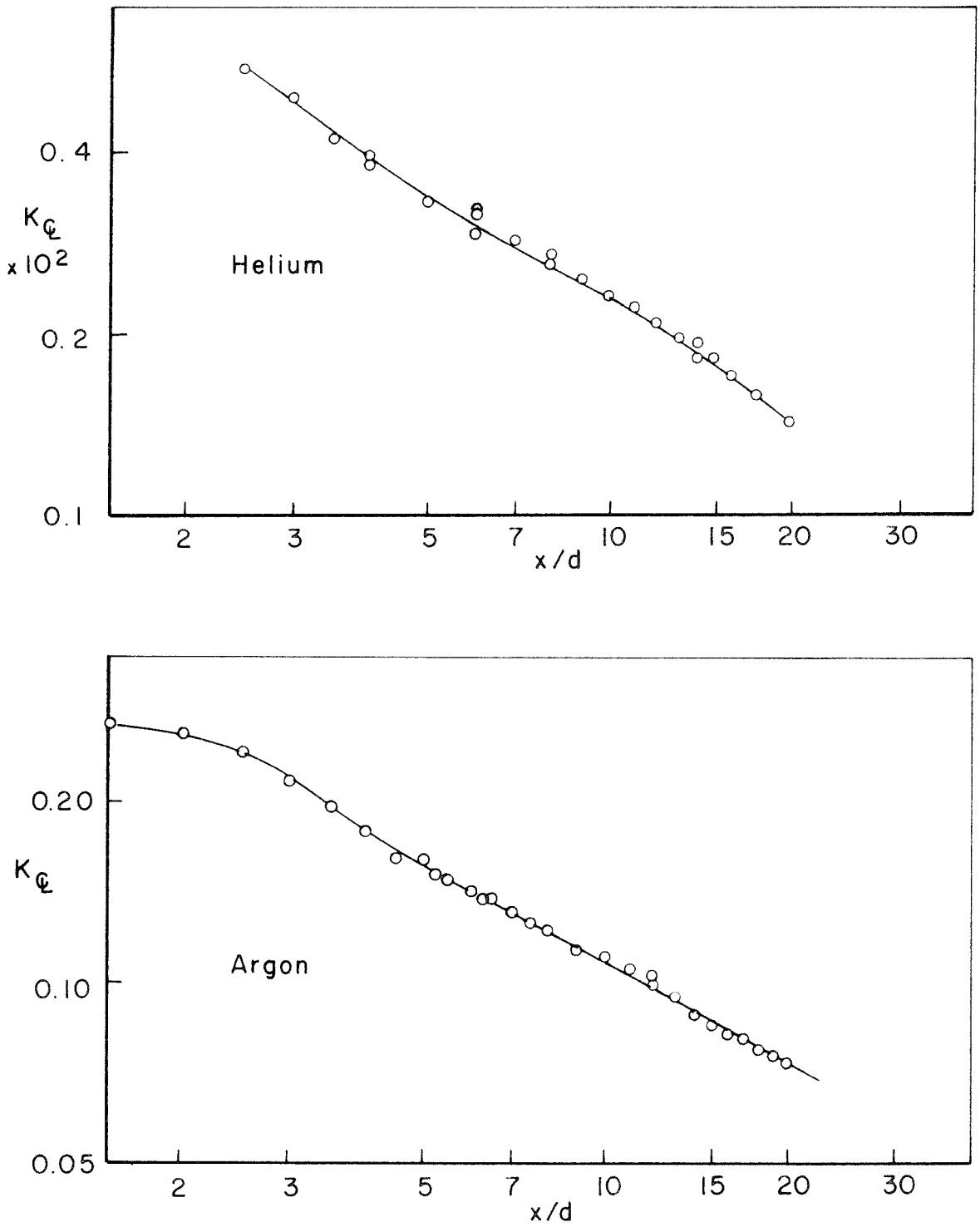

FIG. 21 — VARIATION OF TRACER GAS MASS FRACTION ALONG THE WAKE CENTERLINE AT P_0 = 10 PSIG

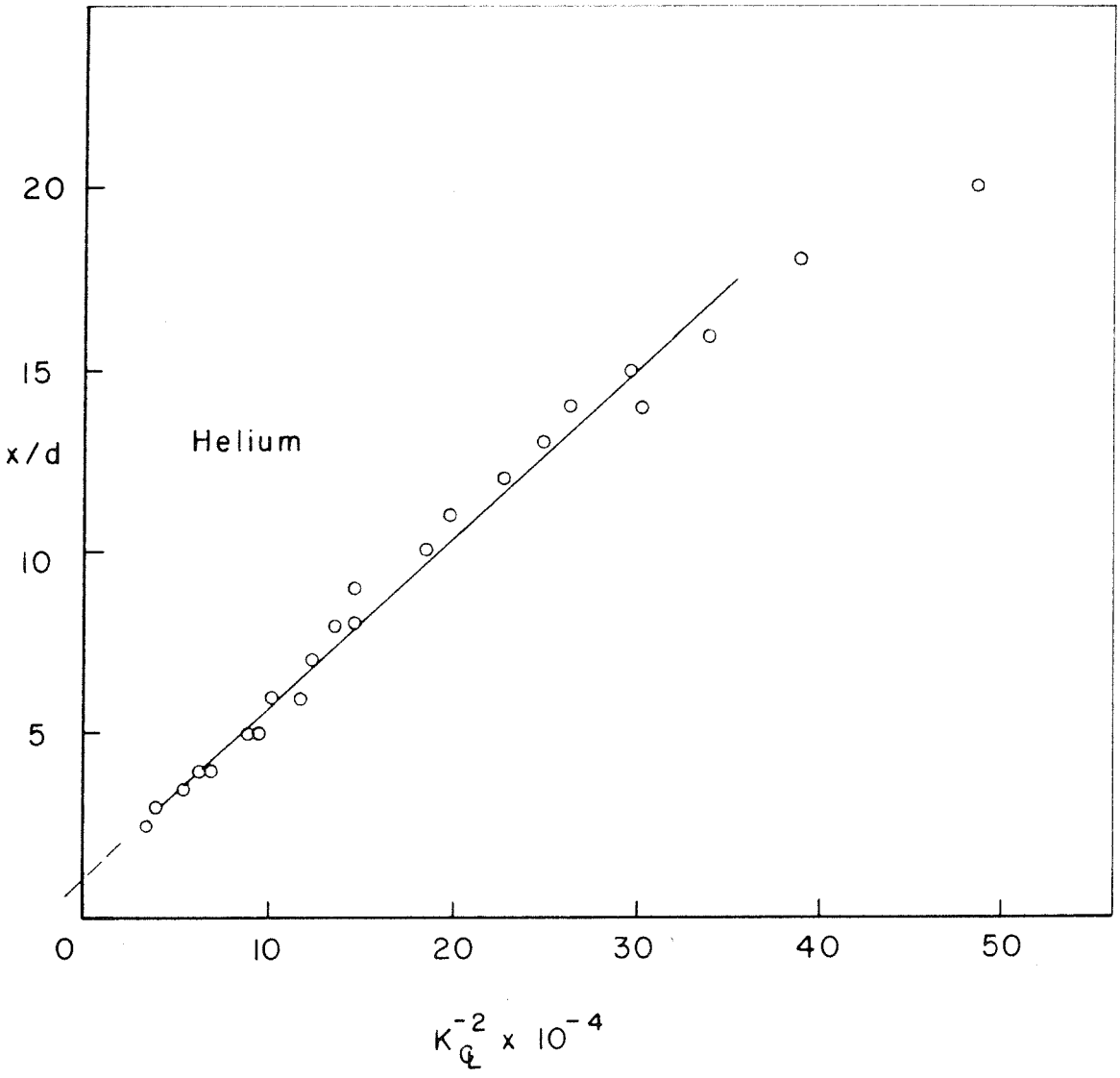

FIG. 22 - PLOT TO DETERMINE VIRTUAL ORIGIN OF HELIUM DIFFUSION AT P_0 = 10 PSIG

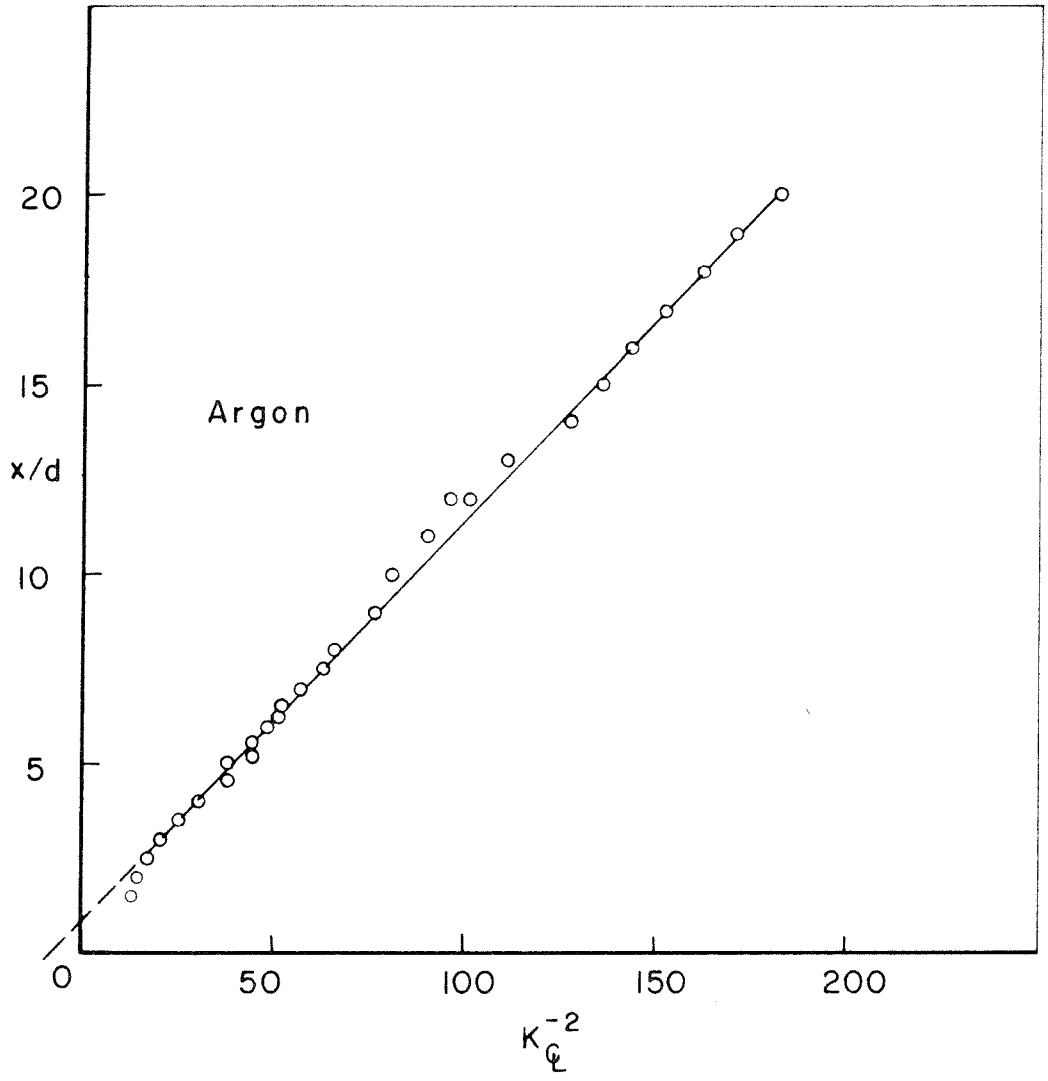

FIG. 23 - PLOT TO DETERMINE VIRTUAL ORIGIN OF ARGON DIFFUSION AT P_0 = 10 PSIG

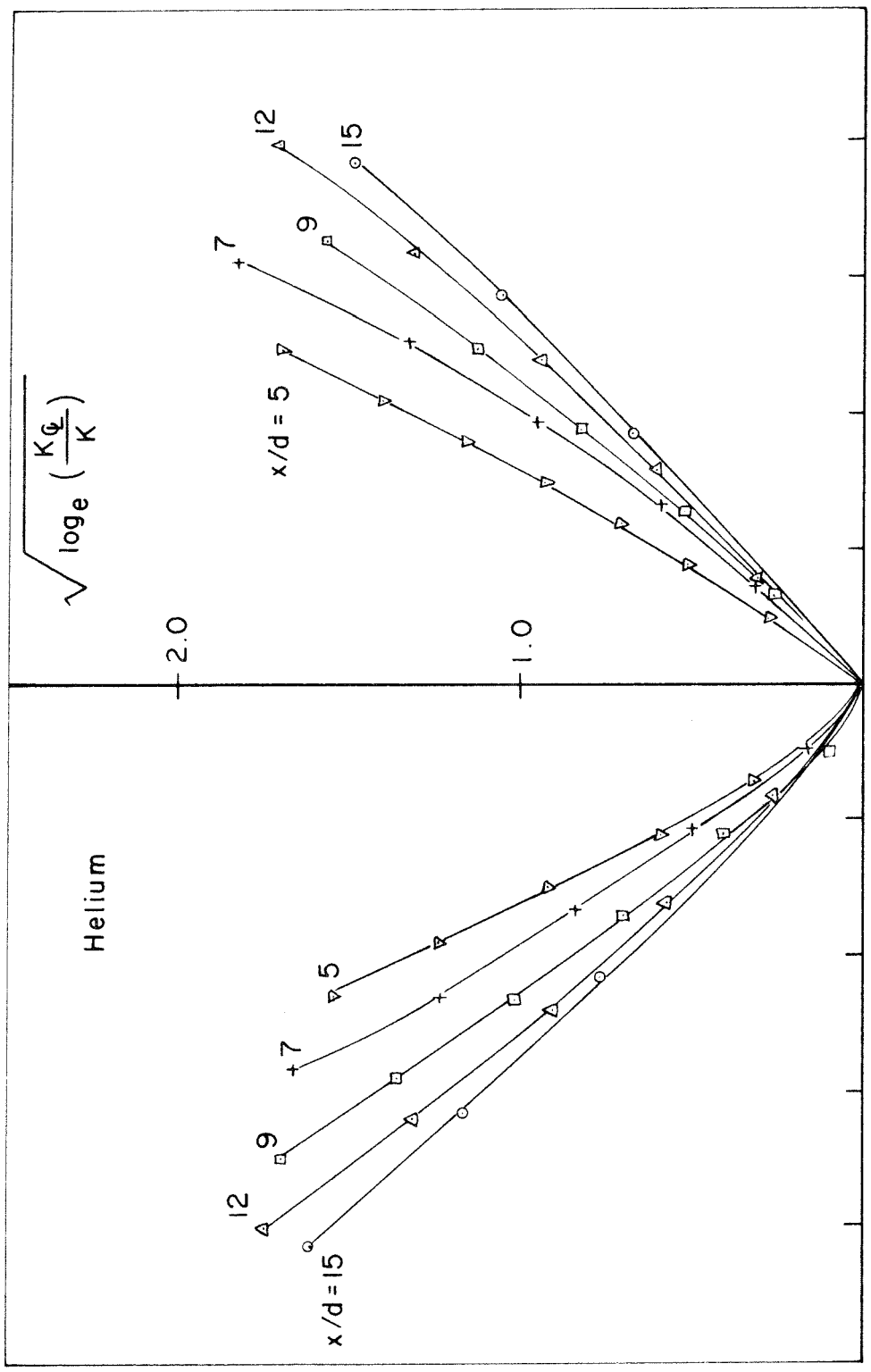

FIG. 24 - PLOT TO DETERMINE $\left(\frac{\partial^2 K}{\partial y^2}\right)_\ell$ FOR HELIUM DIFFUSION AT P_o = 10 PSIG

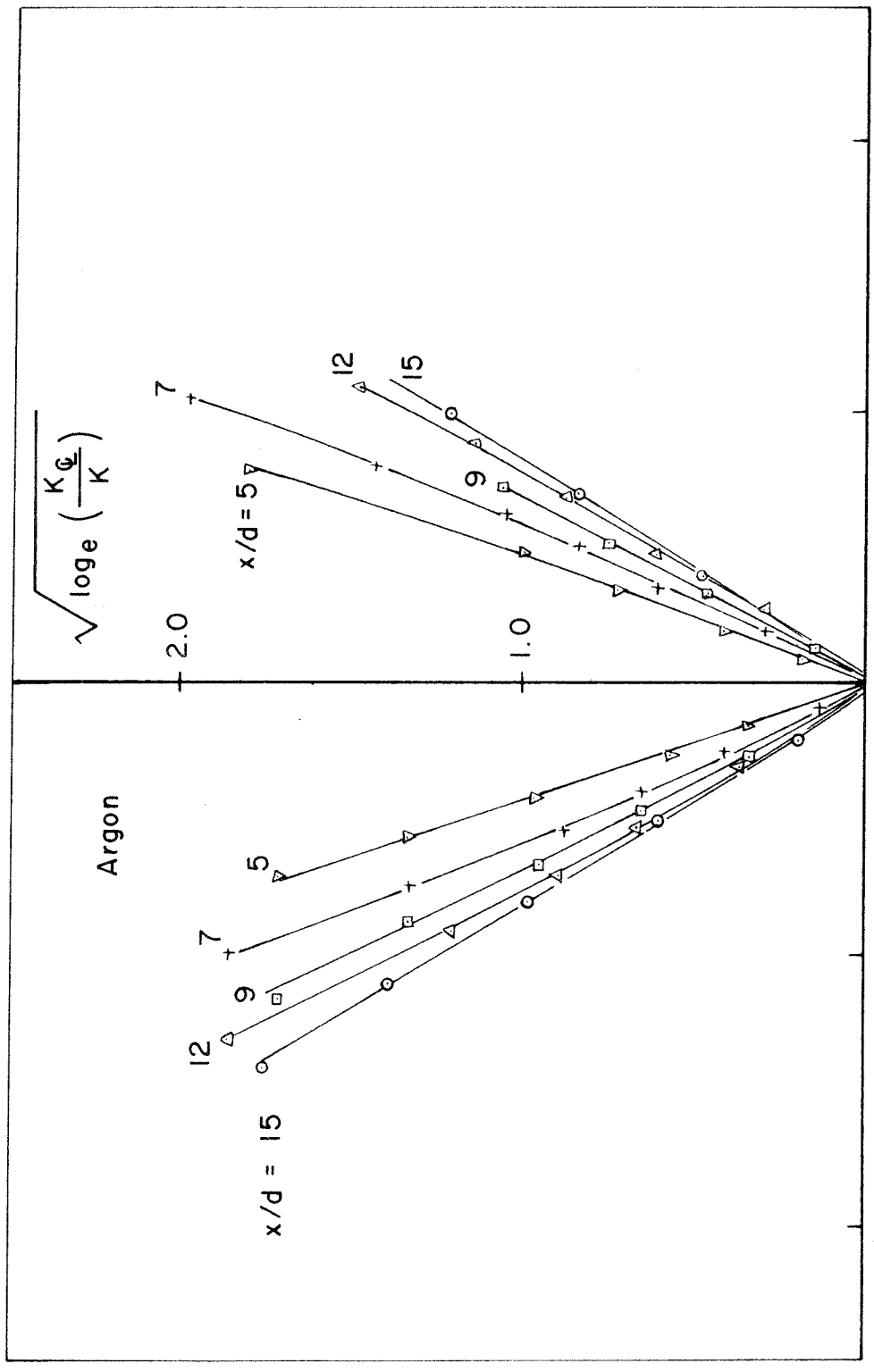

FIG. 25 - PLOT TO DETERMINE $\left(\frac{\partial^2 K}{\partial y^2}\right)_{\mathcal{L}}$ FOR ARGON DIFFUSION AT P_o = 10 PSIG

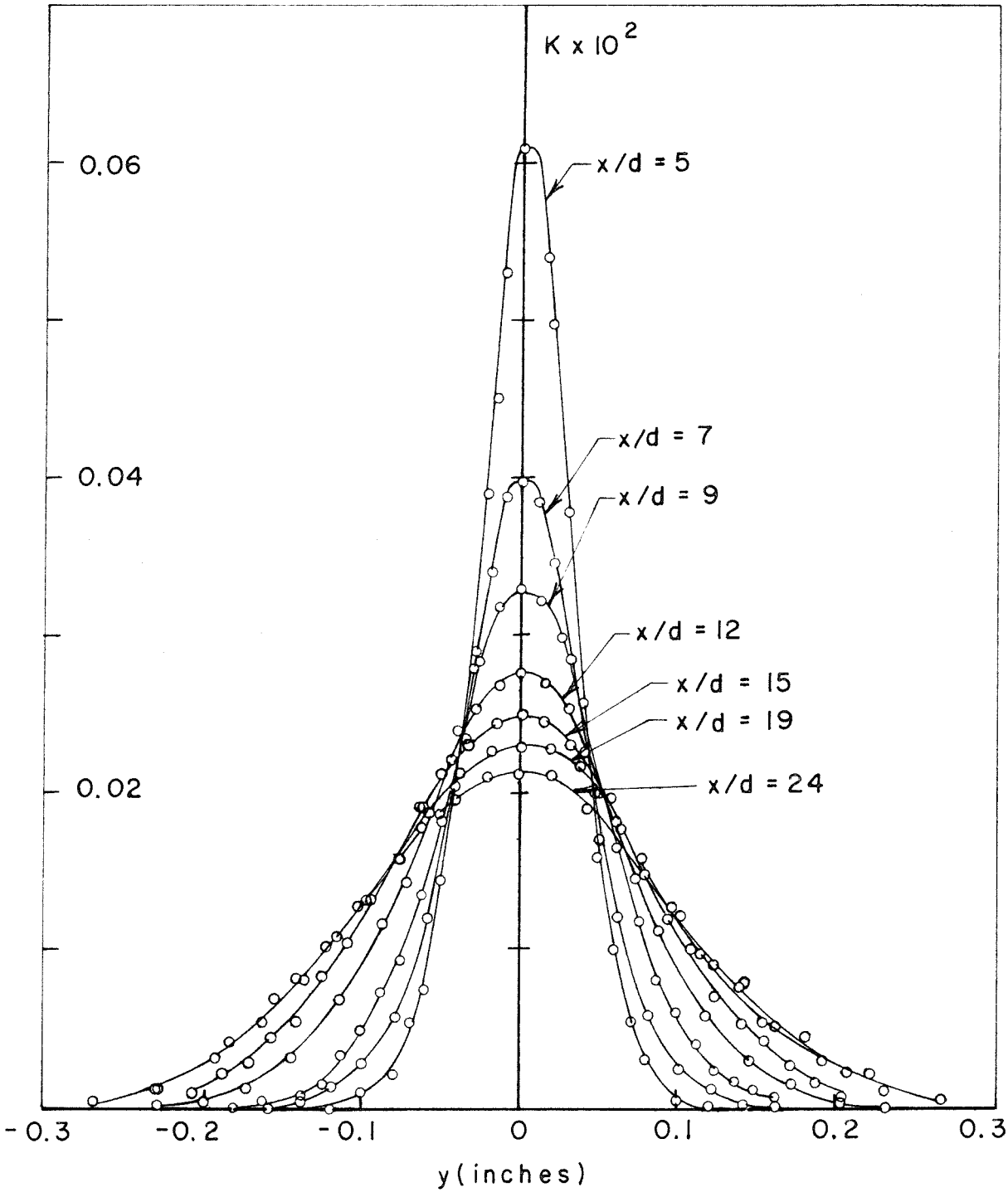

FIG. 26 - HELIUM MASS FRACTION PROFILES AT P_o = 85 PSIG

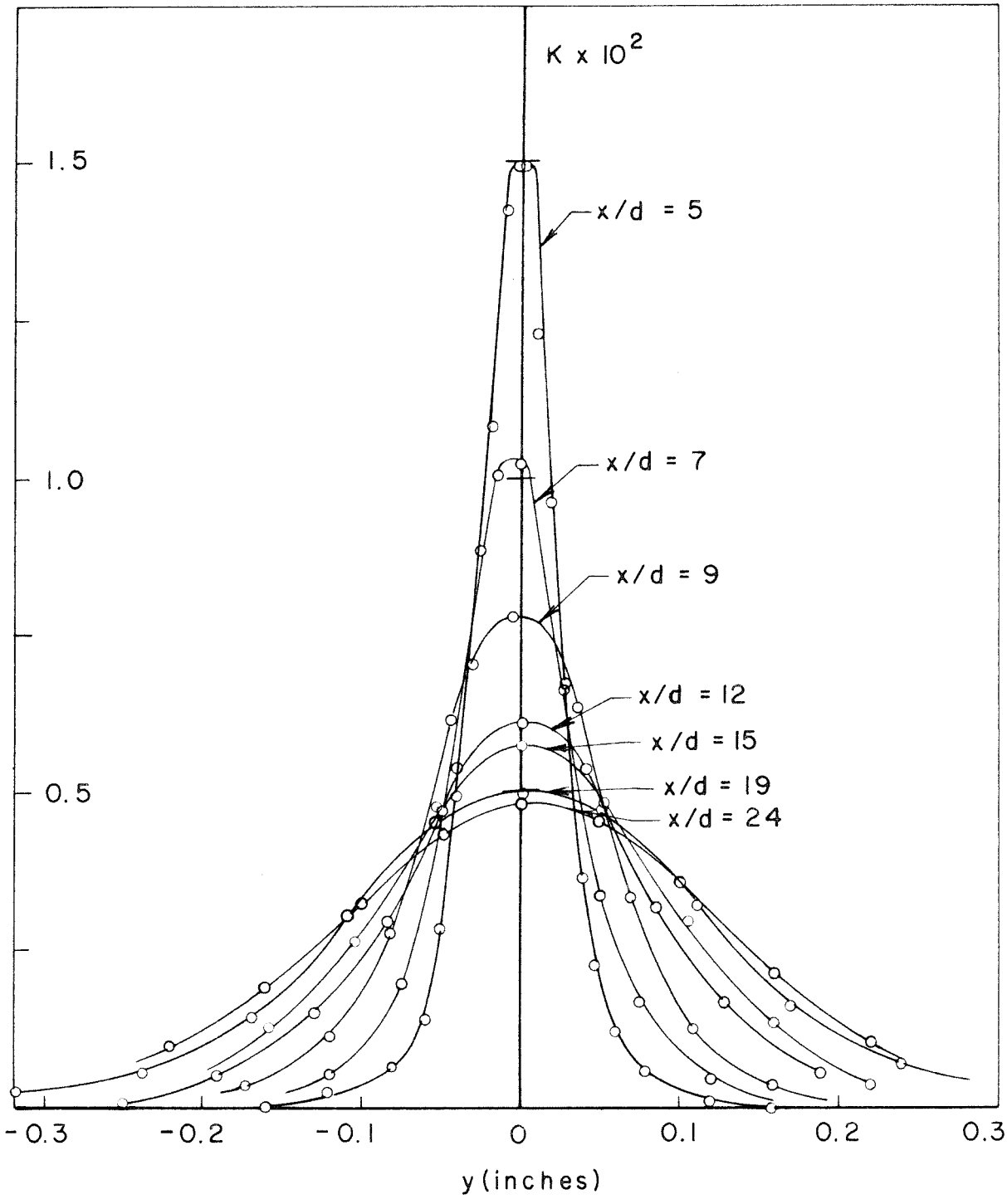

FIG. 27 - ARGON MASS FRACTION PROFILES AT P_0 = 85 PSIG

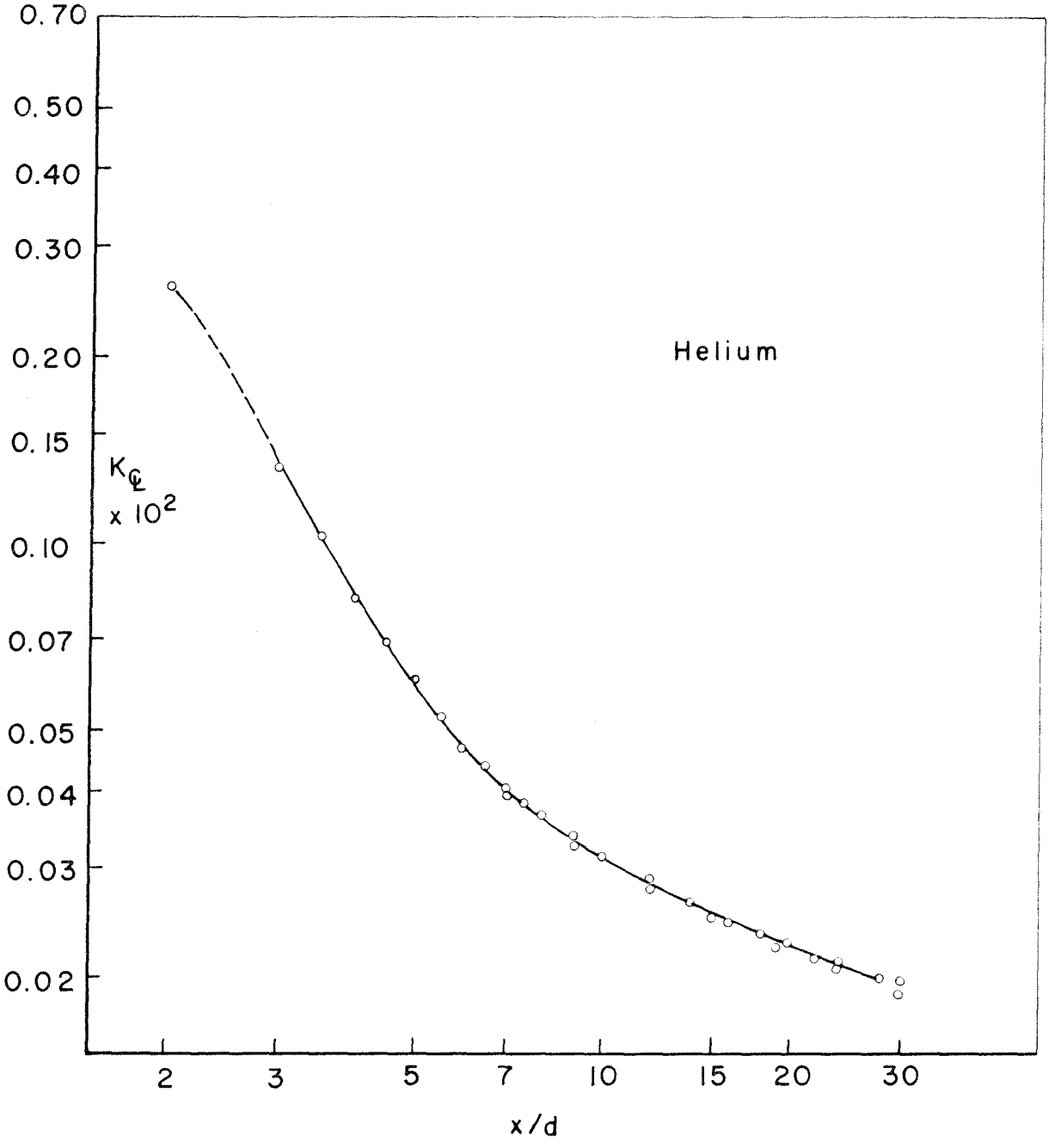

FIG. 28 - VARIATION OF HELIUM MASS FRACTION ALONG THE WAKE CENTERLINE AT P_0 = 85 PSIG

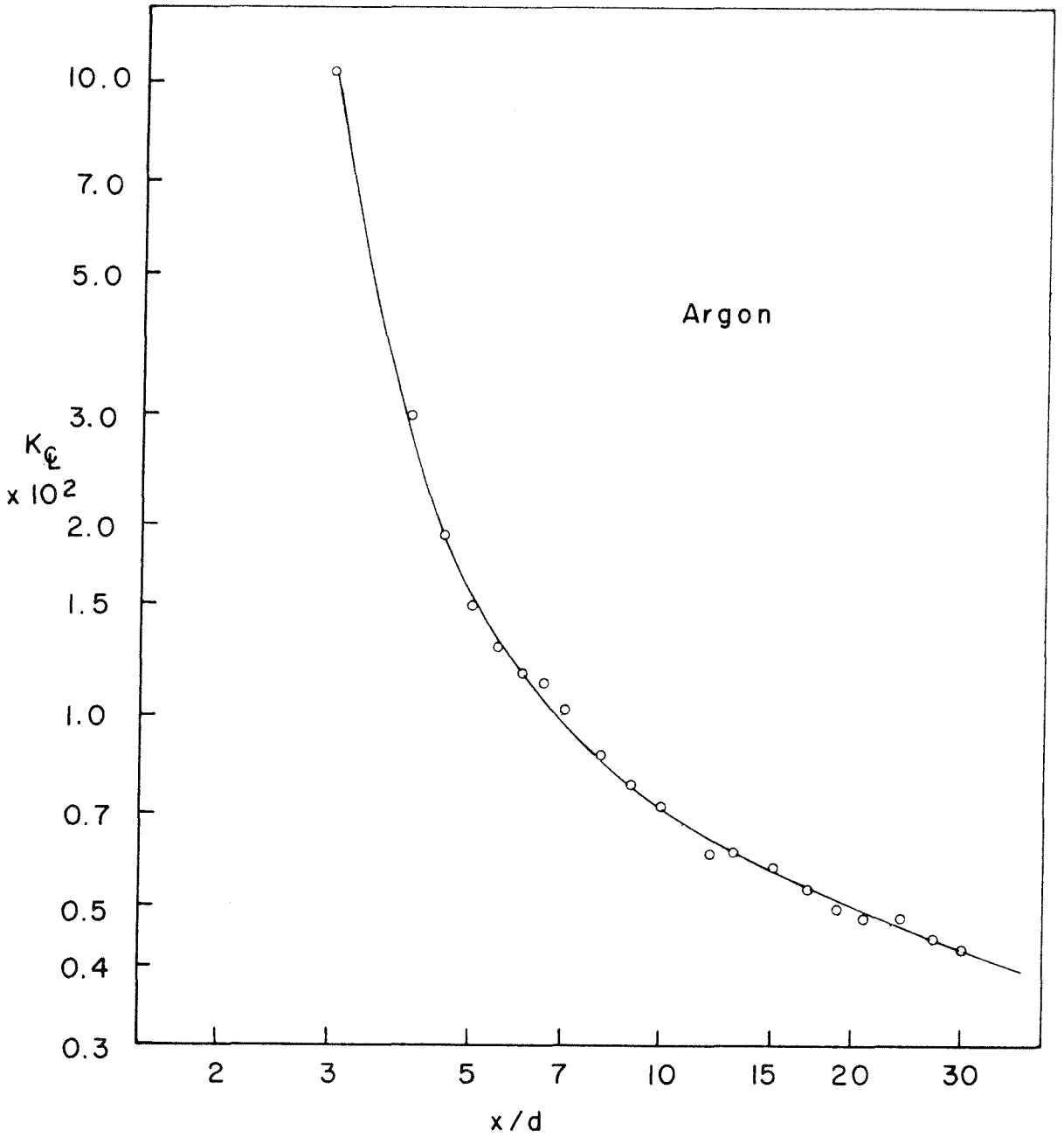

FIG. 29 – VARIATION OF ARGON MASS FRACTION ALONG THE WAKE CENTERLINE AT P_o = 85 PSIG

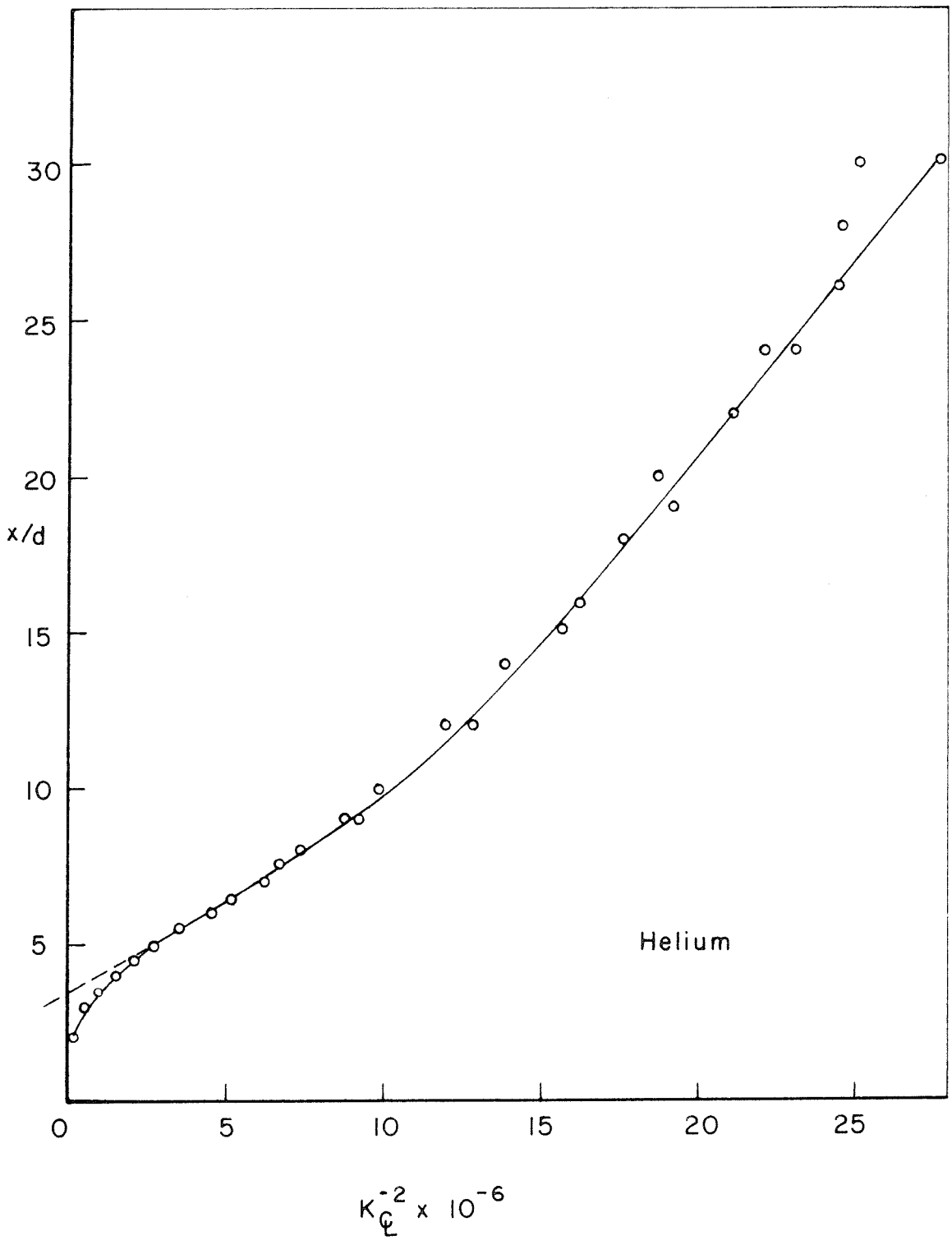

FIG. 30 - PLOT TO DETERMINE VIRTUAL ORIGIN OF HELIUM DIFFUSION AT P_0 = 85 PSIG

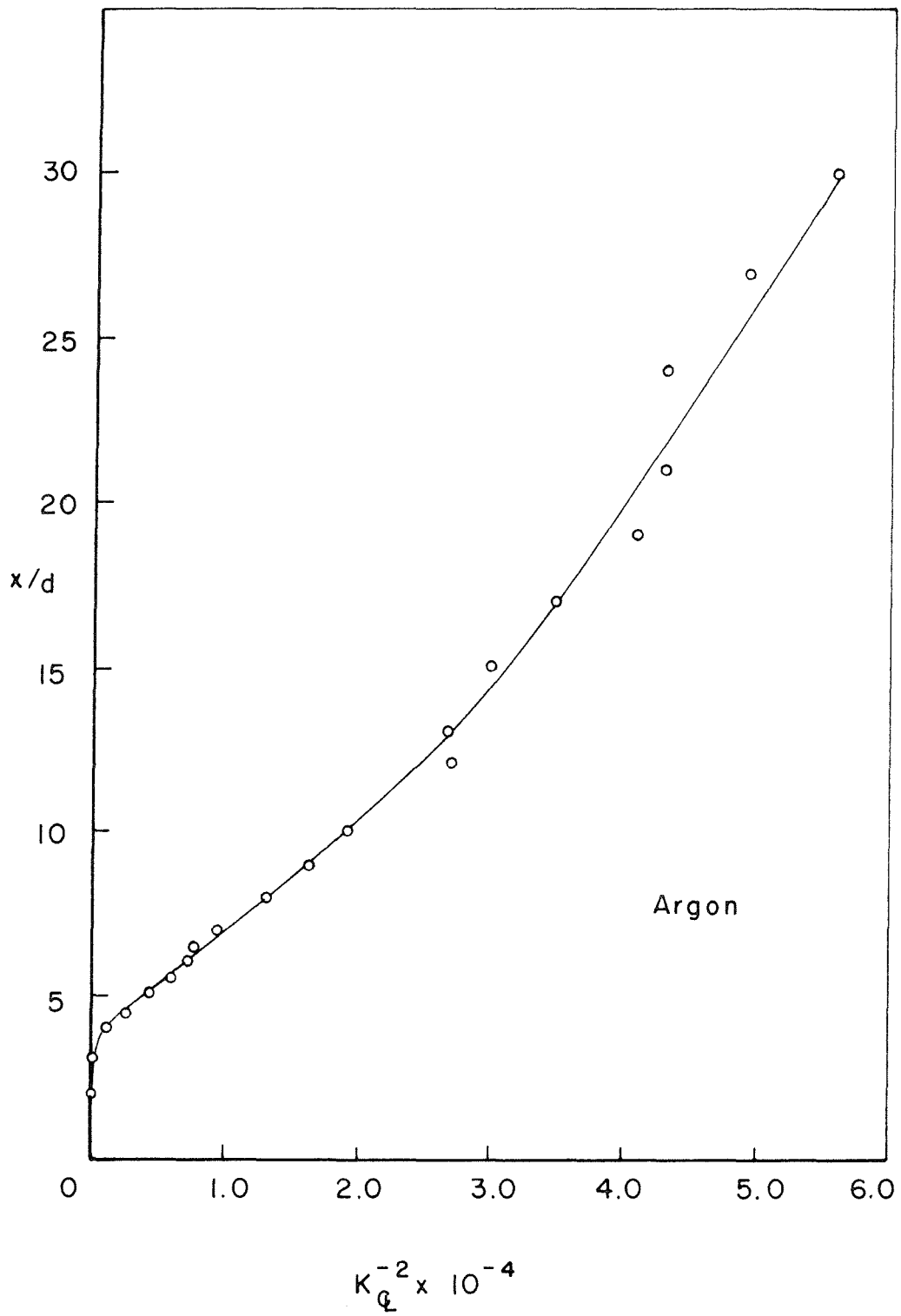

FIG. 31 - PLOT TO DETERMINE VIRTUAL ORIGIN OF ARGON DIFFUSION AT P_0 = 85 PSIG

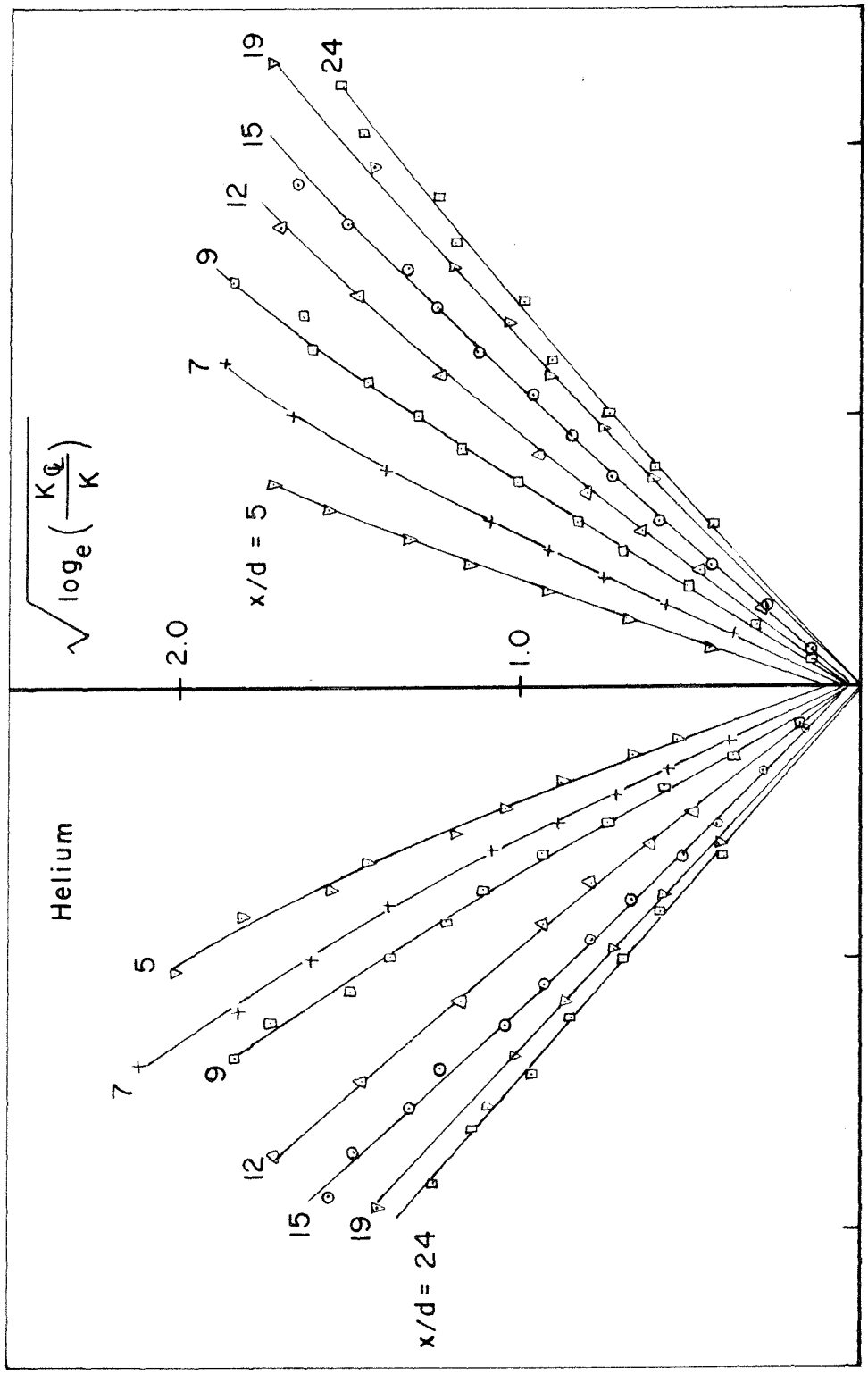

FIG. 32 – PLOT TO DETERMINE $\left(\frac{\partial^2 K}{\partial y^2}\right)_{\mathcal{L}}$ FOR HELIUM DIFFUSION AT $P_o = 85$ PSIG

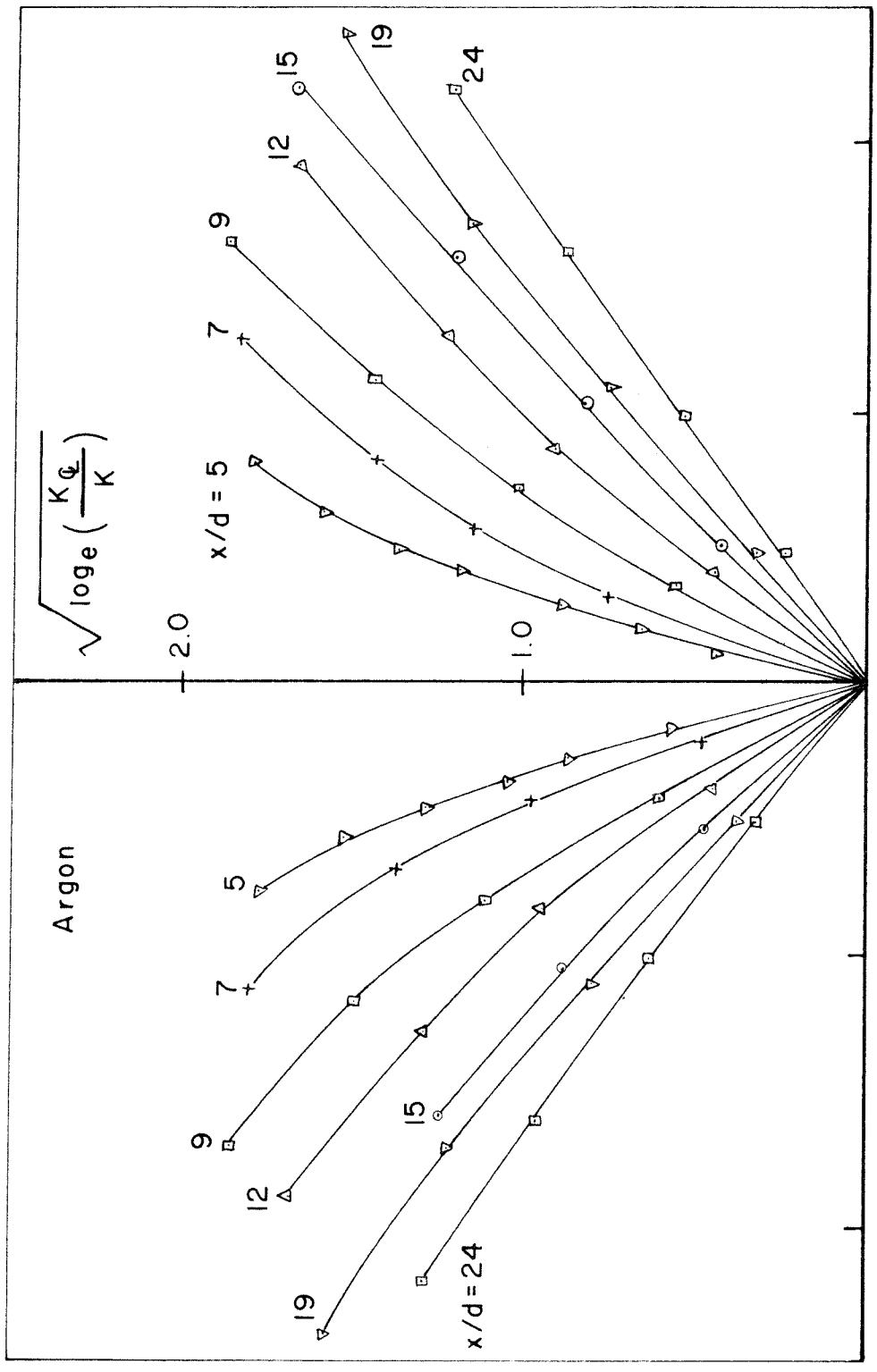

FIG. 33 - PLOT TO DETERMINE $\left(\frac{\partial^2 K}{\partial y^2}\right)_\ell$ FOR ARGON DIFFUSION AT P_o = 85 PSIG

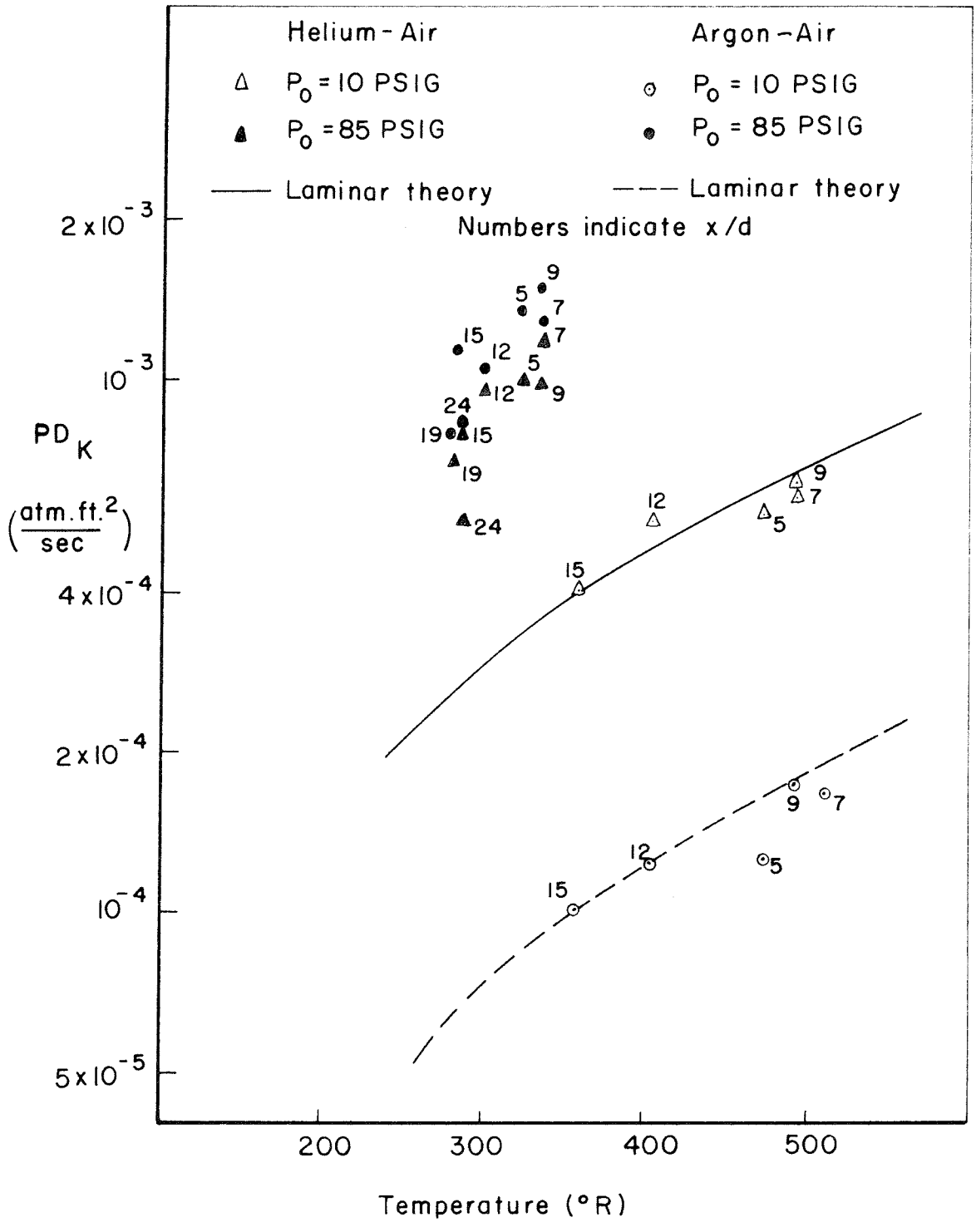

FIG. 34 - COMPARISON OF THEORETICAL AND EXPERIMENTAL DIFFUSION COEFFICIENTS

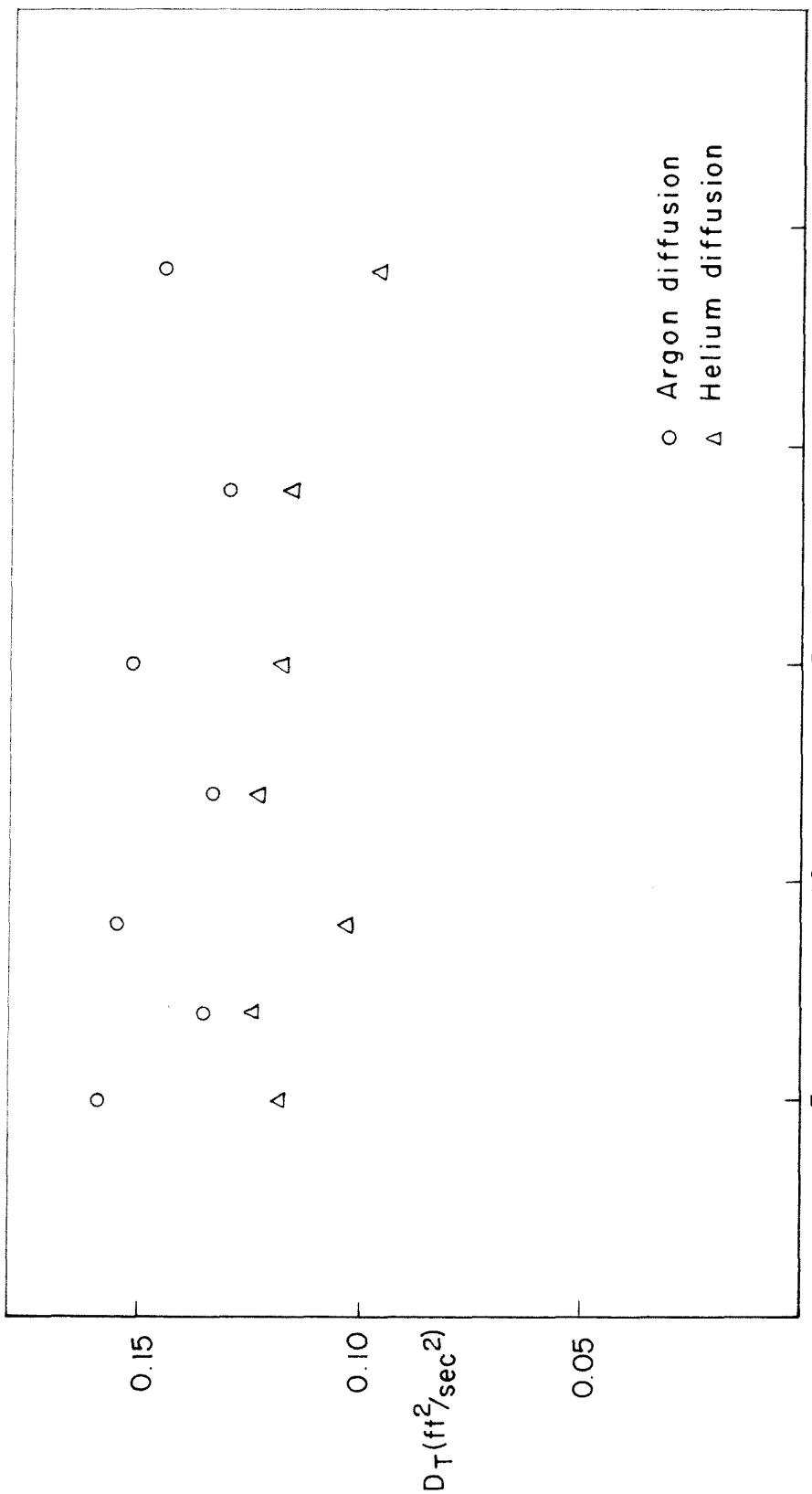

FIG. 35- EXPERIMENTAL DIFFUSION COEFFICIENTS AT P_o = 85 PSIG